UNIVERSITÀ DEGLI STUDI DI GENOVA

Master's degree in Engineering for Natural Risk Management

Title of thesis:

Using remote sensing data to assess cascading effects of wildfires

Supervisor:

Professor Paolo Fiorucci

Candidate:

Farzad Ghasemiazma

Electrical, Electronics and Telecommunication Engineering, and Naval Architecture Department

(DITEN)

December 2022

ACKNOWLEDGMENTS

I would like to express my deepest appreciation to my advisor professor Paolo Fiorucci to give me the opportunity to collaborate with him and Wildfire Risk Management and Forest Conservation Department. The door to Prof. Fiorucci's office was always open whenever I ran into a trouble spot or had a question about my research or writing. This thesis would not have been possible without the help, support, and guidance of him.

I would also like to extend my deepest gratitude to the CIMA research foundation and staff to help me throughout my thesis specially Francesco Silvestro from Hydrology and Hydraulics Department for his instructive and effective suggestions on my thesis. I would like to extend my sincere thanks to Francesco Baghino, and Federico Schiavi for sharing their knowledge and experiences with me and helping me to accomplish my thesis. It has been an amazing experience working between two groups in different departments, Wildfire Risk Management and Forest Conservation Department and Hydrology and Hydraulics Department. This accomplishment would not have been possible without them.

I must thank my parents, my family, and my beautiful girlfriend Pegah, who gave me unreserved support and continuous encouragement during the years of study and the research and writing stages of this thesis.

I would also like to thank all my friends for encouraging and supporting me whenever I needed them.

ABSTRACT

Wildfire is one of the worldwide phenomena which influences the global ecosystem, including vegetation distribution and structure, the carbon cycle, and climate. Cascading effects of fire are an aspect that needed more focus. Cascading effects could be changes in erosion rate, runoff, and water quality. In 2021, Italy was the country's second most affected by fires in terms of burnt area (after Turkey) in Europe, the Middle East, and North Africa. This thesis is aimed at finding a relation between Fireline intensity (resulting from the PROPAGATOR*) and fire severity (resulting from satellite) to use Fireline intensity in the estimation of runoff directly.

The methods for the estimation of cascading effects of wildfire can be categorized into two groups:

- Methods based on in situ measurements (to know soil properties)
- Methods only based on remotely sensed images and data.

The first-mentioned methods are more time and money-consuming, also finding a case study in which the properties of the soil before and after the wildfire is present is too difficult. So, we decided to choose a real fire that occurred on Sardinia Island in Italy, and we computed discharges at three pre-defined points on three different basins (Riu Mannu, Riu Santa Caterina, Pischilappiu a Riola Sardo) based on real data of three years (2017-2020) data to see differences in discharges which are caused by wildfire.

From the literature, three methods based on the modification of SCS_CN have been chosen to modify the CN values of the affected area. These data fed the CONTINUUM* to have hourly discharges in the three mentioned sections.

* Livingston Method
* Cerrelli Method
* Higginson and Jarnecke Method

In this case, the Fireline intensity and the fire severity maps had a low level of correlation (0.26). Then, the fire severity map was used. The results illustrate, depending on the area affected by the fire and the severity of the fire at upstream of the river, catchments have different behavior in the rate of increase. Moreover, the methods which are used also affect the results. High severity and the size of the affected area led to higher discharges. The discharges of sections have increased between 1.2% to 216% depending on severity, area, location of the fire on the basin, method, and amount of discharge.

* Two models developed by CIMA research foundation

CONTENTS

LIST OF TABLES:

LIST OF FIGURES:

1 INTRODUCTION:

Fire is a worldwide phenomenon that appears in the geological record soon after the appearance of terrestrial plants. Fire influences the global ecosystem, including vegetation distribution and structure, the carbon cycle, and climate. Although humans and fire have always coexisted, our capacity to manage fire remains imperfect and may become more difficult in the future as climate change alters fire regimes [1]. Wildfires are one of the most relevant threats to European forests and rural areas, particularly in fire-prone southern Countries. Estimates from the European Forest Fire Information System (EFFIS annual report 2021) show that currently, 2022 is the year with the highest number of fires since 2006. This is in addition to what is expected to be recorded as the most severe drought in Europe in 500 years. The area burnt expanded to over 8 600 km^2 in the EU – the largest area burnt by wildfires since 2006. In the future, under a warmer climate, we expect more severe fire forests, more burned areas more ignitions, and a longer fire season.

Human-caused large-scale forest fires have expanded in the last decades throughout the area, mostly in the EU Mediterranean nations – Spain, Portugal, Italy, and Greece with tremendous social, economic, and environmental Impacts. Moreover, Climate change in the Mediterranean area is causing longer and more extreme summer droughts, as well as the frequent occurrence of Mediterranean woodlands to accommodate them. This is partially associated with climactic characteristics including winter precipitation with moderate temperatures, followed by hot and dry summers.

This climatic regime leads to increased vegetation growth in winter and the presence of highly flammable fuels during the dry summer. Moreover, the frequency of wildfires is expected to increase because of global warming [3].

In 2021, Italy was the country's second most affected by fires in terms of burnt area (after Turkey) and recorded the highest number of fires. The total burnt area of 159 537 ha mapped from 1 422 fires was the highest recorded in over a decade. 90% of the damage occurred in July and August. 15 of the 49 fires exceeded 1 000 ha and the largest (in Sardinia) was over 13 000 ha. Sicily was particularly affected, with 32 of these 49 large fires occurring there[3]. Wildfire, whether natural or generated by humans, changes the landscape abruptly, and for a long time. The elimination of

protecting vegetation, which results in a faster runoff, is one of the most significant effects. In addition, wildfire frequently inhibits soil infiltration, resulting in increased runoff volumes. Post-wildfire runoff events erode stream banks excessively and convey huge loads of silt and debris due to the dramatically altered hydrologic behavior of burnt watersheds [4].

The most critical post-fire cascading impacts of a wildfire are runoff and soil erosion. Studies in Mediterranean ecosystems showed higher rates of runoff after wildfires compared with areas not burned for a long time. Research into post-wildfire effects began in the United States more than 70 years ago and only later extended to other parts of the world. Moody et al.2008 [5] used runoff response, which was measured as the runoff coefficient C, which is equal to the peak discharge per unit drainage area divided by the average maximum 30 min rainfall intensity during each rainstorm. The magnitude of the burn severity was expressed as the change in the normalized burn ratio.

A new burn severity variable, hydraulic functional connectivity Φ was developed and incorporates both the magnitude of the burn severity and the spatial sequence of the burn severity along hillslope flow paths.

Wildfire simulations based on the minimum travel time algorithm were used to characterize wildfire exposure and risk transmission in terms of annual burn probability, flame length, structures exposed, type, and amount of transmission.

Salis et al. 2021 [6] focused on the historical conditions associated with wildfires that occurred in Sardinia in the period 1998–2016, and combined outputs from wildfire simulation modeling with land use, building footprint locations, weather, and historical ignition data.

Authors in this paper investigated the control of post-wildfire runoff by physical and hydraulic properties of soil, hydrologic states, and an ash layer immediately after the following wildfire. Physical and hydraulic property characterization included ash thickness, particle size distribution, hydraulic conductivity, and soil water retention curves. Soil water content and matric potential were measured indirectly at several depths below the soil surface to document hydrologic states underneath the ash layer in the unsaturated zone, whereas precipitation and surface runoff were measured directly. Results showed the importance of including hydrologic conditions and hydraulic properties of the ash layer in post-wildfire runoff generation models [7].

Cerrelli G (2005) [8] developed a spreadsheet, called FIRE HYDRO, to assist NRCS and Forest Service personnel in estimating design peak flows for the burned areas of Montana. FIRE HYDRO is a peak flow analysis tool for 2-, 5-, 10-, 25-, 50-, and 100-year, 24-hour rainfall-runoff events for the pre-fire and post-fire conditions. The required input data includes the following: drainage area (acre); average watershed slope (%); CN; and 2- to 100-year, 6- and 24-hour rainfall depths that are available from NOAA (2008). The 6- and 24-hour rainfall depths are required to determine the SCS rainfall distribution type (Type I, IA, II, or III). The majority of region number 1, including Montana, has Type II, which produces the highest peak flow among the SCS rainfall distribution types.

The Soil Conservation Service Curve Number (CN) method is routinely used to estimate the effects of forest fires on hydrological response. On average, the estimated post-fire CN values for the studied soil-cover complexes increased by about twenty-five units. This study may assist in the improvement of existing post-fire hydrological assessment tools [9].

2 OBJECTIVE OF THE THESIS

Multiple hazardous events are considered cascading when they function as a series of toppling dominoes, such as flooding and landslides that occur after rain over wildfires. Cascading events may begin in small areas but can intensify and spread to influence larger areas.

Wildfires cause hydrometeorological and geomorphic changes that can heighten the susceptibility of burned areas to other hazards; for example, raised soil water repellency after a fire could lead to increased runoff [10]. The lack of vegetation interception and soil infiltration, from the loss of surface roughness from ground litter and hydrophobicity, can shift the rainfall response from infiltration-dominated processes to surface runoff-dominated processes. For instance, watershed impacts due to the recent wildfire caused a Swiss catchment to produce 100-year to 200-year runoff discharges from a 10-year rainfall event due to changes in infiltration capacity [11].

In the first part of this study, the correlation between fire intensity resulting from the application of a propagation model (PROPAGATOR, cit.) and the fire severity was calculated from sentinel-2 data. Moreover, the correlation between topographic characteristics, fire intensity, and fire severity have been shown. This thesis is aimed at comparing the cascading effects of wildfire in terms of runoff by direct runoff estimation specifically using the CN method. Among the different models of estimating the CN value, three methods were used which have been explained in the methodology section. The CN values are manipulated by the results of two scenarios for pre-wildfire and post-wildfire considered and the results of a hydrological model (CONTINUUM[12]) are compared to have an overview of the wildfire effect.

Two models developed by CIMA researchers Foundation have been used in this study PROPAGATOR and Continuum. The PROPAGATOR is a tool designed and activated by researchers of the CIMA Research Foundation. It operates at the prototype level since the summer of 2009. The system is interfaced with the Dewetra platform and aims to provide decision-makers with useful information to implement civil protection activities and to support effective forest fire-fighting activities.

The system is currently being evaluated by the Department of National Civil Protection. The propagator is a model of fire propagation, which can simulate the behavior of a single fire triggered in each area of the territory.

The system can provide maps of the probability of fire propagation by predicting the dynamics of the flame front and defining emergency scenarios. The propagator is based on the availability of detailed maps of vegetation cover, a digital model of the terrain, and the representation of the wind field [13].

The Continuum model is useful in forecasting and risk reduction because it can provide the basin's responses to meteorological stresses, especially in the event of intense events. But the great utility of Continuum is also expressed in the possibility of being implemented in areas with poor ground instrumentation and in the possibility of calibrating the model concerning variables such as soil moisture or soil temperature that are rarely present in other models. available. Continuum also has features that make it applicable to diverse types of basins, different climates, and highly anthropized territories with the presence of hydraulic works (dams) that can play a significant role in reducing the effects of floods [12]. This model is aimed at balancing the need to reproduce the physical processes with the practical goal of avoiding over-parameterization. The model is designed to be implemented in different contexts with a special focus on data-scarce environments, e.g., with no streamflow data [14].

3 STATE OF THE ART

Wildfires cause hydrometeorological and geomorphic changes that can heighten the susceptibility of burned areas to other phenomena such as floods, landslides, and soil erosion. Also, Drought increased the likelihood of wildfires, which burned vegetation and raised the likelihood of increased surface runoff, soil erosion, and hillslope failures [15], [16]. Over short and long timescales, wildfire (i.e., uncontrolled, or naturally occurring fire) can be an important, if not the major, cause of hydrological and geomorphological change in fire-prone landscapes [15].

This thesis is aimed to focus on the effects of wildfires on runoff immediately after the wildfire. The research was applied to the Montiferru fire that occurred in Sardinia in July 2021. An important difficulty in this study was deciding the length of the post-fire period used for the estimation of the post-fire CN values.

Another important issue that this article intends to address is finding a correlation between Fireline intensity and fire severity and possibility to modify CN values based on fire intensity. Previous studies have shown that the period necessary for hydrological processes recovery to the pre-fire conditions depends on the type of species existing before the fire because each species has its specific recovery rate. The amount of remaining litter and vegetation cover, which is related to the burn severity, also has an important role in post-fire runoff and erosion rates, and in the recovery time of burned soils [17]–[20]. Furthermore, the vegetation recovery and the hydrological response recovery may be constrained by other factors, which are common in Mediterranean countries, such as water shortage and generally harsh meteorological and hydrological conditions [21]. The hydrological processes recovery period may range from 1 year in optimal conditions to five or even ten years after the wildfire in dry areas [20]–[23]. Sardinia contains a high density of urban interfaces, recreational values, and highly valued agricultural areas that are increasingly being threatened by severe wildfires [24]. In this study, a short-term effect of wildfire on the soil characteristics and CN has been considered i.e., the situation before vegetation recovery.

Postfire CN values based on three methodologies have been obtained. I have compared four different results to get knowledge about different runoffs. The first result is related to pre-fire conditions, and this is compared with three post-fire conditions considering different methodologies for changing the value of the CN.

4 THE PROPOSED METHODOLOGY

In the literature, three main methods for modification of the CN value were found. The adjusted post-fire CN decreases the time of concentration parameter, resulting in the faster routing of peak discharge through the affected basins [25].

4.1 Livingston

They provided a guideline to choose the post-fire runoff numbers with a range of values as seen below (Table 4.1.1). They used computed CNs and compared pre-and post-fire CNs for 31 small (0.12 to 2.5 mi^2) subbasins in the Los Alamos area, New Mexico, and 24 small (0.11 to 2.3 mi^2) subbasins affected by the 2002 Long Mesa Fire at Mesa Verde National Park, Colorado. To classify the soil, burn severity of the whole watershed/basin, they used Wildfire Hydrologic Impact (WHI), based on the percentage of high and moderate soil burn severity (Table 4.1.2 and Figure 6.1.1) and a general relation between pre- and post-fire CN ratio (Figure 4.1.2)[26].

Soil burn severity	Estimation CN
Unburned	55 to 75
Low	80 to 83
Moderate, without water-repellent soils	87
Moderate, with water-repellent soils	89
High, without water-repellent soils	92
High, with water-repellent soils	95

Table 4.1.1 Post-fire corresponding curve number for various burn severities

Percentage of subbasins with a high soil burn severity	Wildfire Hydrologic Impact classification
0-6	Low
7-48	Moderate
49-80	Severe

Table 4.1.2 Variations in Wildfire Hydrologic Impact (WHI) due to high soil burn severity

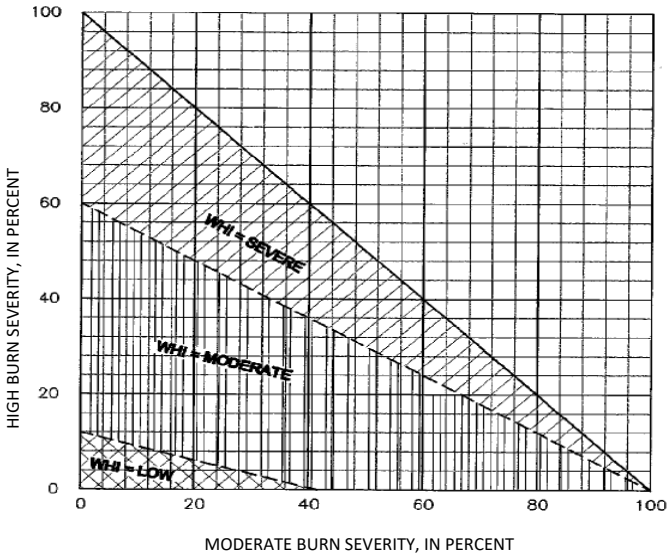

Figure 4.1.1 WHI for small burned subbasin as a function of soil burn severity

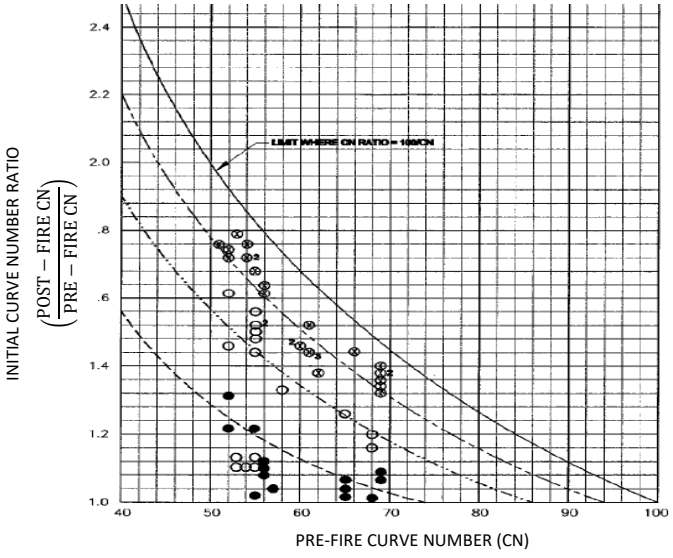

Figure 4.1.2 General relation between pre-fire and post-fire CN ratio for indicated WHI

4.2 Cerrelli

He provided a guideline to select post-fire CN based on burn severity and hydrologic soil grouping specific to the Bitterroot National Forest wildfires (Table 4.2.1). He did not find appropriate CNs in his initial search of the literature for CN values for burned areas in southwestern Montana. Consequently, Montana NRCS engineers created a guideline based on the existing NRCS CN/ land use table (Table 4.2.2 and Table 4.2.3) [8].

Soil Burn Severity	**Sub-Category**	**Estimation CN**
High	HSG* A	64
	HSG B	78
	HSG C	85
	HSG D	88
Moderate	-	Use cover type** in Fair condition
Low and unburned	North and East facing slopes	Use cover type in good condition
	South and West facing slopes	Use cover type between Fair and Good condition
Any	Water repellent soils	94

Table 4.2.1 Post-fire CNs for various burn severities based on the bitterroot national forest

* Hydrologic soil groups

** From Table 4.2.2 and Table 4.2.3

Cover description		Curve number for HSG			
Cover type	**Hydrologic condition**	**A**	**B**	**C**	**D**
Bare soil	-	77	86	91	94
Pasture, grassland, or range-continuous forage for grazing	Poor	68	79	86	89
	Fair	49	69	79	84
	Good	39	61	74	80
Meadow-continuous grass, protected from grazing and generally mowed for hay	-	30	58	71	78
Brush-weed-grass mixture with brush the major elements	Poor	48	67	77	83
	Fair	35	56	70	77
	Good	30	48	65	73
Woods-grass combination (orchard or tree farm)	Poor	57	73	82	86
	Fair	43	65	76	82
	Good	32	58	72	79
Woods	Poor	45	66	77	83
	Fair	36	60	73	79
	Good	30	55	70	77
Farmsteads-building, lanes, driveways, and surrounding lots	-	59	74	82	86

Table 4.2.2 Runoff CNs for other agricultural lands (USDA)

Cover description		Curve number for HSG			
Cover type	**Hydrologic condition**	**Ac**	**B**	**C**	**D**
Herbaceous-mixture of grass, weeds, and low-growing brush, with brush the minor element	Poor	-	80	87	93
	Fair		71	81	89
	Good		62	74	85
Oak-aspen-mountain brush mixture of oak brush aspen, mountain mahogany, bitter brush. maple, and other brush	Poor		66	74	79
	Fair		48	57	63
	Good		30	41	48
Pinyon-juniper, pinyon, juniper, or both. grass understory	Poor		75	85	89
	Fair		58	73	80
	Good		41	61	71
Sagebrush with grass understory	Poor		67	80	86
	Fair		51	63	70
	Good		35	47	55
Desert shrub-major plants include saltbush greasewood, creosote bush, blackbrush, bursage, palo Verde, mesquit and cactus	Poor	63	77	85	88
	Fair	55	72	81	86
	Good	49	68	79	84

Table 4.2.3 Runoff CNs for aid and semiarid rangelands (USDA)

4.3 Higginson and Jarnecke

Since there are limited studies and guidelines for choosing CNs for post-fire conditions, BAER team members often use simple rules of their own. Details on these rules are found in the NRCS CN Methods section. For example, in the Salt Creek BAER Hydrology Special Report, they used the following rules to determine post-fire CNs (maximum value is 100).

- Low burn severity
- Moderate burn severity
- High burn severity

- CN = Pre-fire CN + 5
- CN = Pre-fire CN + 10
- CN = Pre-fire CN + 15

5 APPLICATION TO A CASE STUDY AREA

5.1 Case study

Sardinia is the second-largest island in the Mediterranean Sea (after Sicily and before Cyprus), with an area of 24,100 km^2. It is situated between 38° 51' and 41° 18' latitude north (respectively Isola del Toro and Isola La Presa) and 8° 8' and 9° 50' east longitude (respectively Capo dell'Argentiera and Capo Comino).

Figure 5.1.1 National and regional parks of Sardinia

To the west of Sardinia is the Sea of Sardinia, a unit of the Mediterranean Sea; to Sardinia's east is the Tyrrhenian Sea, which is also an element of the Mediterranean Sea. Over 600,000 hectares (1,500,000 acres) of the Sardinian territory is environmentally preserved (about 25% of the island's territory). The island has three national parks and Ten regional parks (Figure 7.1.1)[27], [28]. An active wildfire in Sardinia's Oristano area (Montiferr regional park) has triggered localized evacuations as of July 26. A state of emergency has been declared in Sardinia due to the fire. The blaze has burned approximately 9,955 hectares (Figure 7.1.2) (24,600 acres) of state and private land, damaged several buildings, and displaced hundreds of people in the towns of Cuglieri, Scano Montiferru, and Sennariolo. Authorities evacuated around 1,500 people across Sardinia, but since early July 26, some have been allowed to return. At least 7,500 emergency workers have been deployed to help with evacuations and battle the blaze [29].

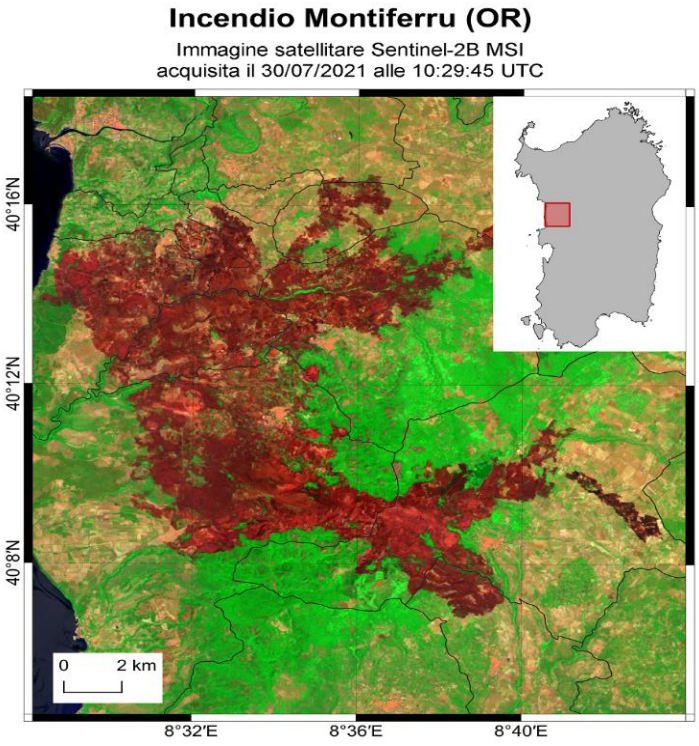

Figure 5.1.2 Study area

6 MATERIAL AND METHODS:

6.1 Wildfire part:

In papers dealing with post-fire studies, there has been a disturbing number that has acknowledged problems in terminology associated with Fireline Intensity and fire severity. First, let us have an overview of the definition of these two terms. Fireline Intensity describes the physical combustion process of energy release from organic matter, while the term burn severity has replaced fire severity, although the metric is remarkably similar and is based on the loss of organic matter in the soil and aboveground organic matter conversion to ash [30].

Fireline Intensity, together with fire residence time (heating duration), vegetation properties, topography, substrate, and climate control the loss or decomposition of aboveground and belowground organic matter [31], meaning that each fire can burn with different severity levels. To perform a fire severity assessment, both field and remote sensing approaches can be used [32]. Spaceborne and airborne multispectral sensors detect changes in the composition and moisture of aboveground vegetation and char/ash deposition by measuring modifications of the recorded electromagnetic spectrum, concerning pre-fire conditions [33]– [35].

In this way, a consistent description of the most used indices was provided by Mallinis et al [34], indices considering Near Infrared (NIR) and Shortwave Infrared (SWIR) spectral regions are widely employed because they are less sensitive to atmospheric contamination, while they quantify vegetation removal, charcoal deposition, and reduction of the canopy moisture and canopy shadow, which lead to a reduced NIR and higher SWIR post-fire reflectance, respectively, compared to healthy vegetation. One of the most used indices exploiting these bands is the differenced Normalized Burned Ratio index (dNBR), based on the subtraction of the NBR post-fire from the NBR pre-fire. [33], [36]– [38]. The dNBR data are grouped according to threshold-based classification models to represent different fire severity levels. This index has been successfully evaluated worldwide, as well as in the Mediterranean area, showing a fair accuracy concerning field measurements of fire severity [32].

Knowledge about meteorological systems, triggering rainfall, relationships between fire severity topography and the hydrological response of watersheds, and the magnitude of flow processes are still poor. For this reason, there is a concrete need to collect these types of data in post-fire settings occurring in Italy.

To simulate the fire event in July in Montiferru regional park and to calculate the Fireline Intensity, the PROPAGATOR model was used. PROPAGATOR is a stochastic cellular automaton model for forest fire spread simulation, conceived as a rapid method for fire risk assessment. The model uses high-resolution information such as topography and vegetation cover considering several types of vegetation. Input parameters are wind speed and direction and the ignition point. The fire spread probability depends on vegetation type, slope, wind direction and speed, and fuel moisture content. The fire-propagation speed is determined through the adoption of a Rate of Spread model. The PROPAGATOR model is a quasi-empirical stochastic CA model based on a raster implementation, which discretizes the space into a grid composed of square cells of arbitrary length Dx = Dy = L.

The cell size reflects the resolution in space of the analysis and the results. In this work, L has been fixed to 20 m, allowing PROPAGATOR to give high-resolution output, fundamental for reproducing the middle-sized Mediterranean fires object of the following sections. At the center of the cells, information on the elevation and vegetation cover are interpolated from the raster's input (Digital Elevation Model and land-cover raster files) [39].

Data Retrieval for PROPAGATOR:

- Ignition Point, Wind Speed, and Wind Direction
- Fire Fighting Actions
- Burned Area Geometries
- Land-Cover Files
- Orography Files (DEM)

The burnt severity intends to discriminate in the scorched area various levels of damage. This is a critical aspect of fire effects assessment since burn severity is closely related to regeneration patterns. For most fires, burn severity is not included in the fire reports, since it requires a great field effort. The service offered in the Preview project comprises two temporal scales: Short-term damage assessment and Long- term damage assessment. The former is intended for quick evaluation of fire effects, and the latter for more detailed analysis. Quick assessment is required for updating strategic planning concerning fire suppression resources, and to evaluate the functioning of fire danger indices. Long-term evaluation is expected to provide a more detailed analysis of the effects of fire on vegetation and soil, providing guidelines for planning post-fire measures [40].

Burn severity has typically been evaluated in situ after fire by measuring soil characteristics, such as char depth, organic matter loss, and color, along with aboveground vegetation consumption, scorch, mortality, and recovery [41]. In recent years to generate a burn severity map for the assessment of the areas affected by wildfires the Normalized Burn Ratio (NBR) is used, as it was designed to highlight burned areas and estimate burn severity.

The Near Infrared (NIR) and Shortwave Infrared (SWIR) spectral regions are relevant for detecting burned areas: NIR highlights changes in canopy cover and brightness of leaf burn [39], whereas SWIR detects changes in landscape dryness [42]. After a fire, with the destruction of vegetation, the NIR reflectance strongly decreases and, on the other hand, the SWIR reflectance increases due to the fire's removal of water-retaining vegetation [43]. Other important spectral regions for BA detection are the Red and Red-Edge because they are linked to strong absorption of the chlorophyll content in plants [44], [45]. For mapping burned areas, some algorithms use a combination of NIR and SWIR spectral regions, although some spectral indices combining only SWIR spectral regions or Red/Red-edge and NIR spectral regions have been developed as well.

Figure 6.1.1 compares burned area signature with healthy vegetation, remarking how areas devastated by fire have an extremely high reflectance in the SWIR wavelengths and low reflectance in the NIR.

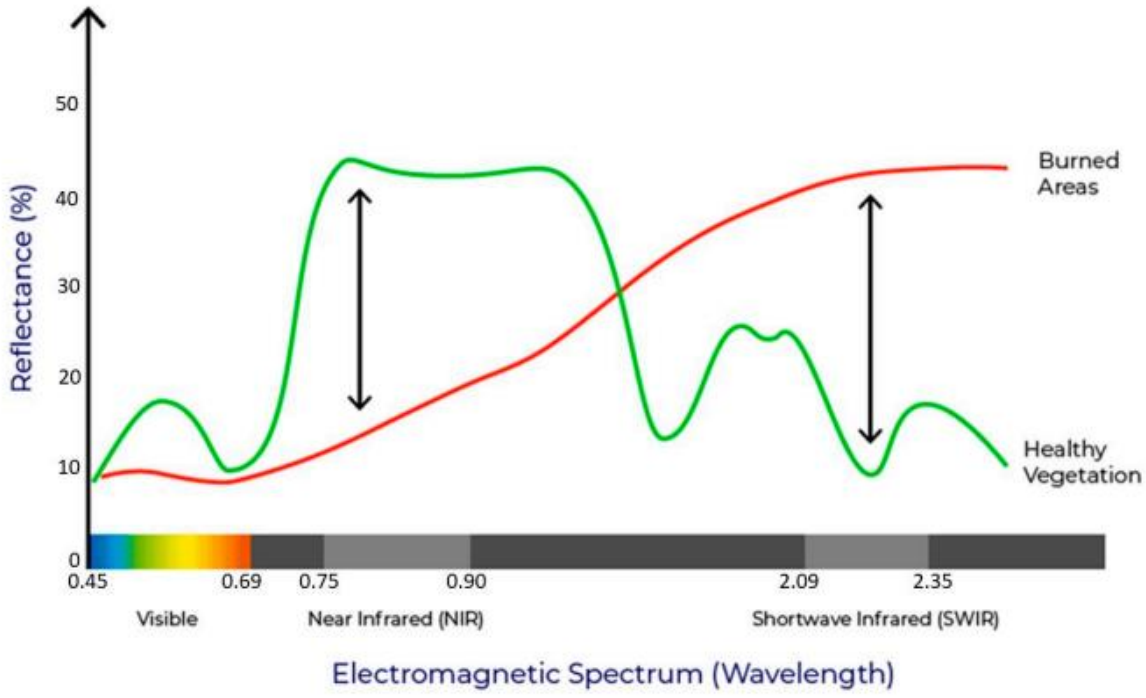

Figure 6.1.1 Comparison of the spectral response of healthy vegetation and burned areas

Fire severity assessment was carried out using satellite data acquired by Multi-Spectral Instrument (MSI) on board Sentinel-2 and the operational land imager (OLI) sensor onboard Landsat 8. This sensor measures the Earth's reflected radiance over thirteen spectral bands spanning from visible and NIR to SWIR bands, at different spatial resolutions [46].

To identify the burned area and characterize fire severity, the dNBR spectral index was calculated using the following equations:

- NBR = NIR - SWIR /NIR + SWIR
- $dNBR = NBR_{pre\text{-}fire} - NBR_{post\text{-}fire}$

The most suitable bands to detect burned areas for Sentinel-2 and Landsat-8 data are bands (B8-B12) and (B5-B7) respectively [47]. The dNBR can be classified according to the burn severity ranges proposed by the United States Geological Survey (USGS) (Figure 6.1.2)

Severity Level	dNBR Range (scaled by 10^3)	dNBR Range (not scaled)
Enhanced Regrowth, high (post-fire)	-500 to -251	-0.500 to -0.251
Enhanced Regrowth, low (post-fire)	-250 to -101	-0.250 to -0.101
Unburned	-100 to +99	-0.100 to +0.99
Low Severity	+100 to +269	+0.100 to +0.269
Moderate-low Severity	+270 to +439	+0.270 to +0.439
Miderate-high Severity	+440 to +659	+0.440 to +0.659
High Severity	+660 to +1300	+0.660 to +1.300

Figure 6.1.2 Burn severity classes and thresholds proposed by USGS. Color coding established by UN-SPIDER

The command to categorize the severity of dNBR raster files in the raster calculation tool in QGIS:

"IF ("dNBR@1" >= -500 AND "dNBR@1" < -251, 1,if ("dNBR@1" >= -250 AND "dNBR@1" < -101,2,if ("dNBR@1" >= -100 AND "dNBR@1" < 99,3,if ("dNBR@1" >= 100 AND "dNBR@1" < 269,4,if ("dNBR@1" >= 270 AND "dNBR@1" < 439,5,if ("dNBR@1" >= 440 AND "dNBR@1" < 659,6,if ("dNBR@1" >=660 AND "dNBR@1" < 1300, 7,0)))))))"

After using the above-mentioned command for our severity maps, we obtained the following categorized severity maps:

- Enhanced regrowth, high [1]
- Enhanced regrowth, low [2]
- Unburned [3]
- Low severity [4]
- Moderate-low severity [5]
- Moderate-high severity [6]
- High severity [7]

6.2 Runoff part

Recently, there has been an increase in natural as well as man-made disasters in the world. Hydrological extremities caused by human activities, increased urbanization, global warming, and weather change can be attributed to the dramatic rise in global flood risks [48]. According to EM-DAT 2022, floods, being the most commonly occurring natural disaster, have caused approximately 122,000 fatalities on a global scale since 2000. Remote sensing technologies acquire data about objects and infrastructure on the surface of the Earth without being in direct contact by using various recording instruments [49]. Therefore, it is helpful in areas where no physical or close contact is possible [50]– [52]. Examples of such technologies include SAR, space-based imaging platforms, and satellites. This technique helps in faster data collection [53].

CONTINUUM is a hydrological model developed by CIMA Foundation researchers to reproduce the flow of water within a basin, i.e., how much water passes in each section of a river or lake. Continuum is a model capable of working both in the pre-event analysis and forecasting phase and in the monitoring phase for control at the same time as the event. CIMA Foundation's choice to study its model arises from the need to develop a model with a reduced number of parameters able to take advantage of all the information available via satellite.

In this thesis, suitable inputs for CONTINUUM have been prepared to have the opportunity of taking advantage of the model. Then the discussion about the results of the cascading effects (in this case runoff) would have been done.

7 RESULTS AND DISCUSSION:

7.1 Fireline Intensity data:

Thanks to PROPAGATOR Six scenarios for wildfire were simulated with different boundary conditions:

A. Result with arbitrary boundary conditions in 23 hours (Figure 7.1.1)
   - Ignition point: [40°07'11.9"N 8°39'06.0"E (DMS), 40.119969, 8.651672(DD)]
   - Wind speed: 80 [km/h]
   - Wind direction: 135°
   - Moisture content: 15 %
   - Time limit: 1380 min

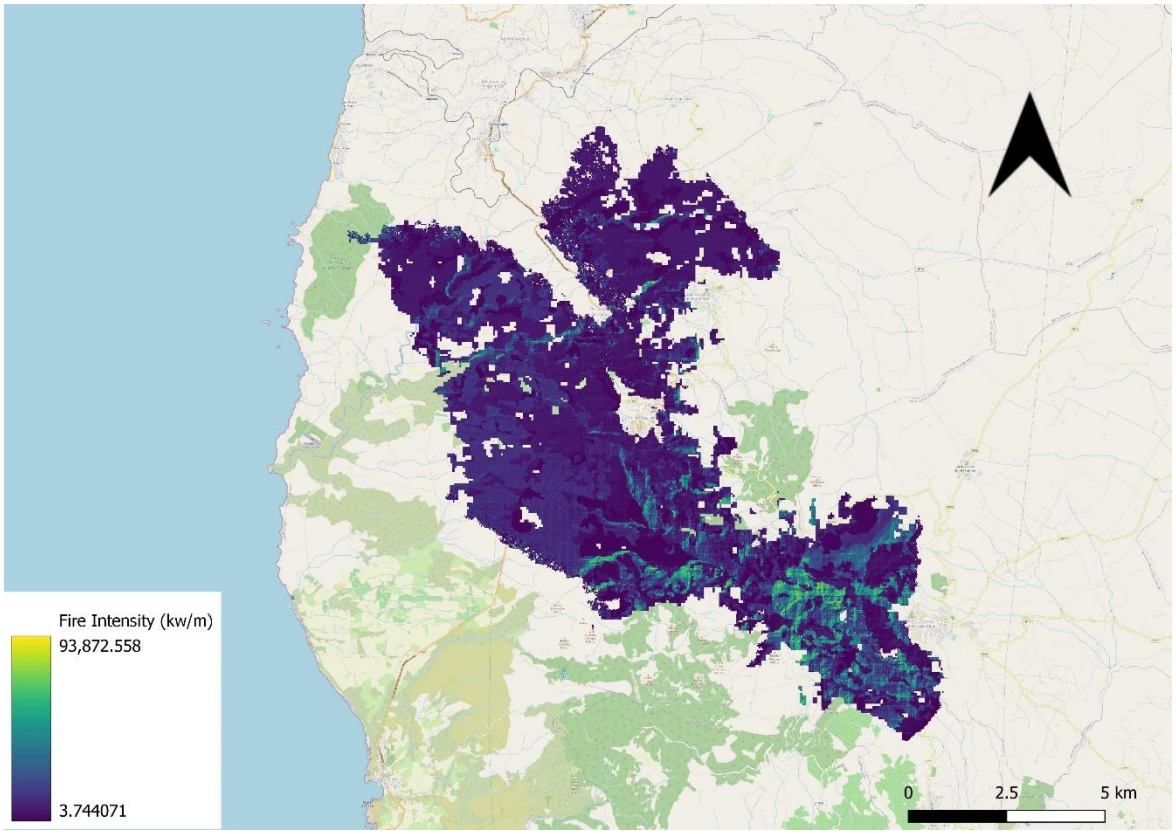

Figure 7.1.1 Result with arbitrary boundary conditions in 23 hours

B. Result with fifteen lines (firefighting action) in 48 hours (Figure 7.1.2)

- Ignition point: [40°07'11.9"N 8°39'06.0"E (DMS), 40.119969, 8.651672(DD)]
- Wind speed: 80 – 85[km/h]
- Wind direction: 160° - 150°
- Moisture content: 15 %
- Time limit: 360 min - 2880 min

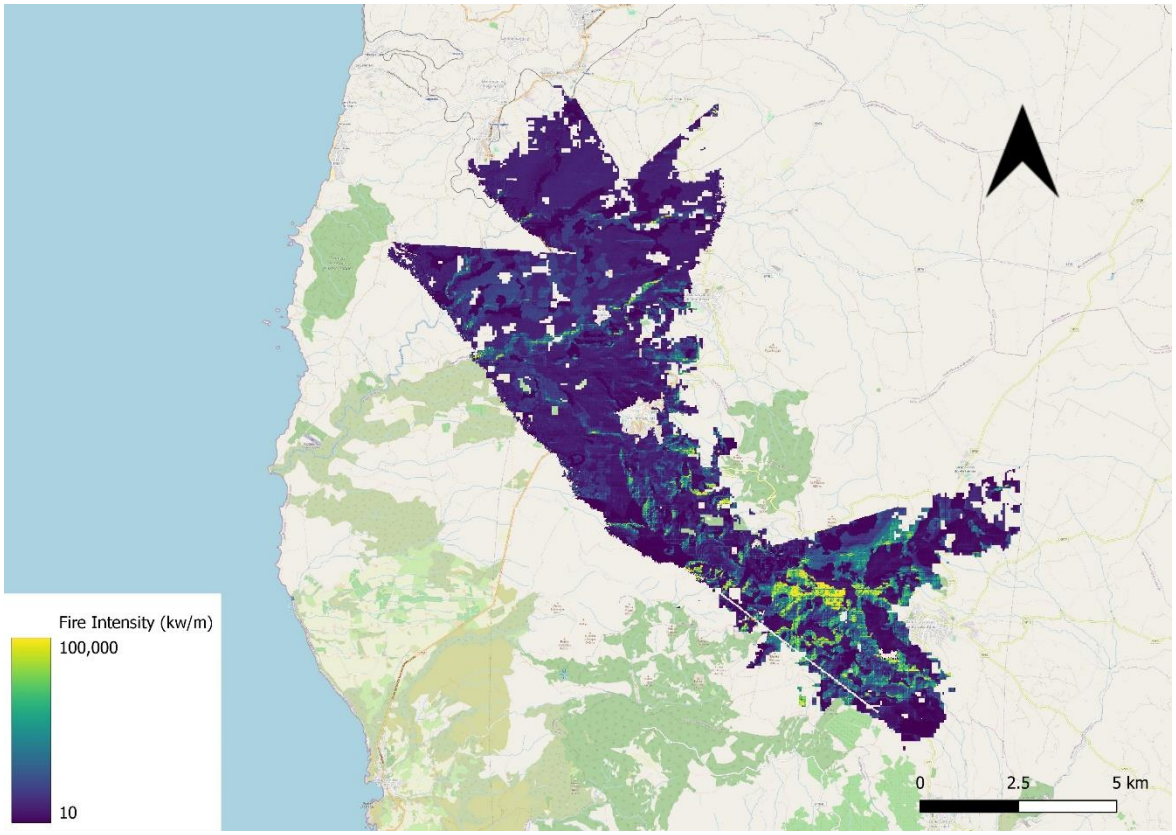

Figure 7.1.2 Result with 15 lines (firefighting action) in 48 hours

C. Result with modified vegetation and 2 lines of firefighting action (Figure 7.1.3)

- Ignition point: [40°07'11.9"N 8°39'06.0"E (DMS), 40.119969, 8.651672(DD)]
- Wind speed: 35 – 30[km/h]
- Wind direction: 130° - 150°
- Moisture content: 10 %
- Time limit: 780 min - 3600 min

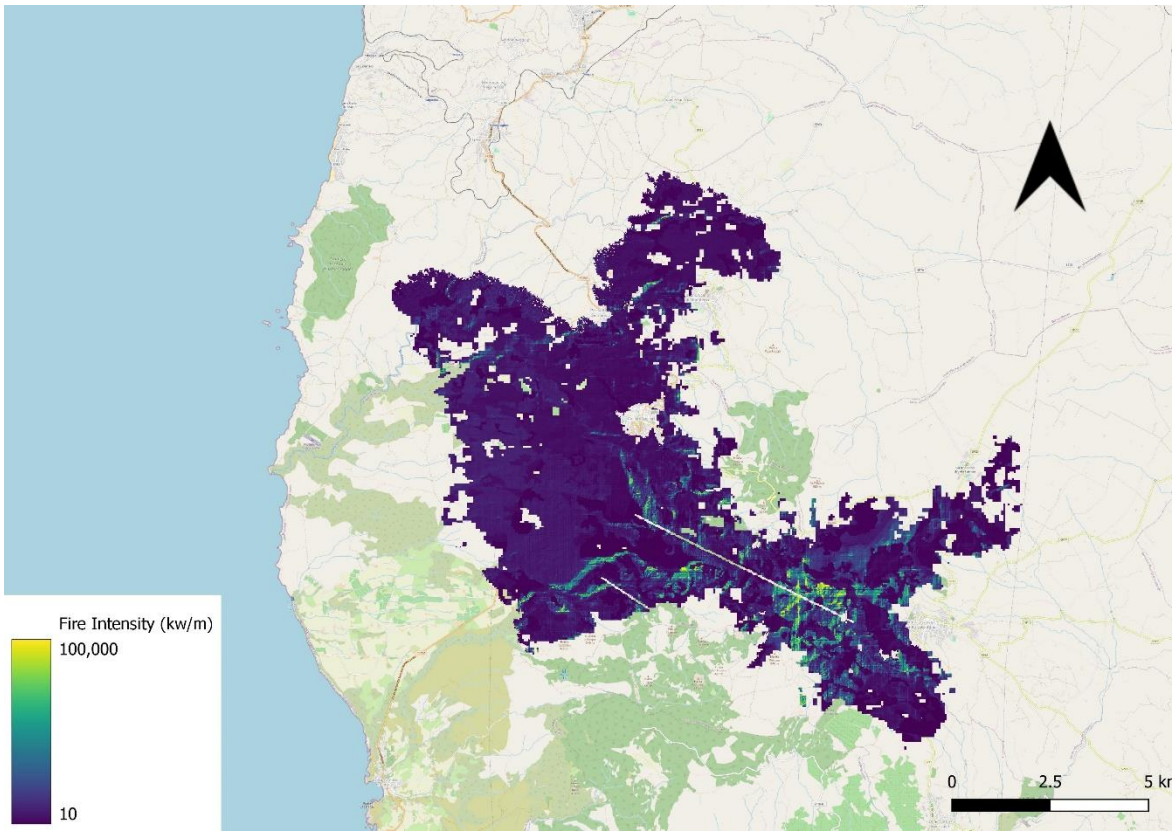

Figure 7.1.3 Result with modified vegetation and 2 lines (firefighting action)

D. Result with modified vegetation and fifteen lines (firefighting action) (Figure 7.1.4)

- Ignition point: [40°07'11.9"N 8°39'06.0"E (DMS), 40.119969, 8.651672(DD)]
- Wind speed: 40 – 35 [km/h]
- Wind direction: 135° - 150°
- Moisture content: 10 %
- Time limit: 780 min - 3600 min

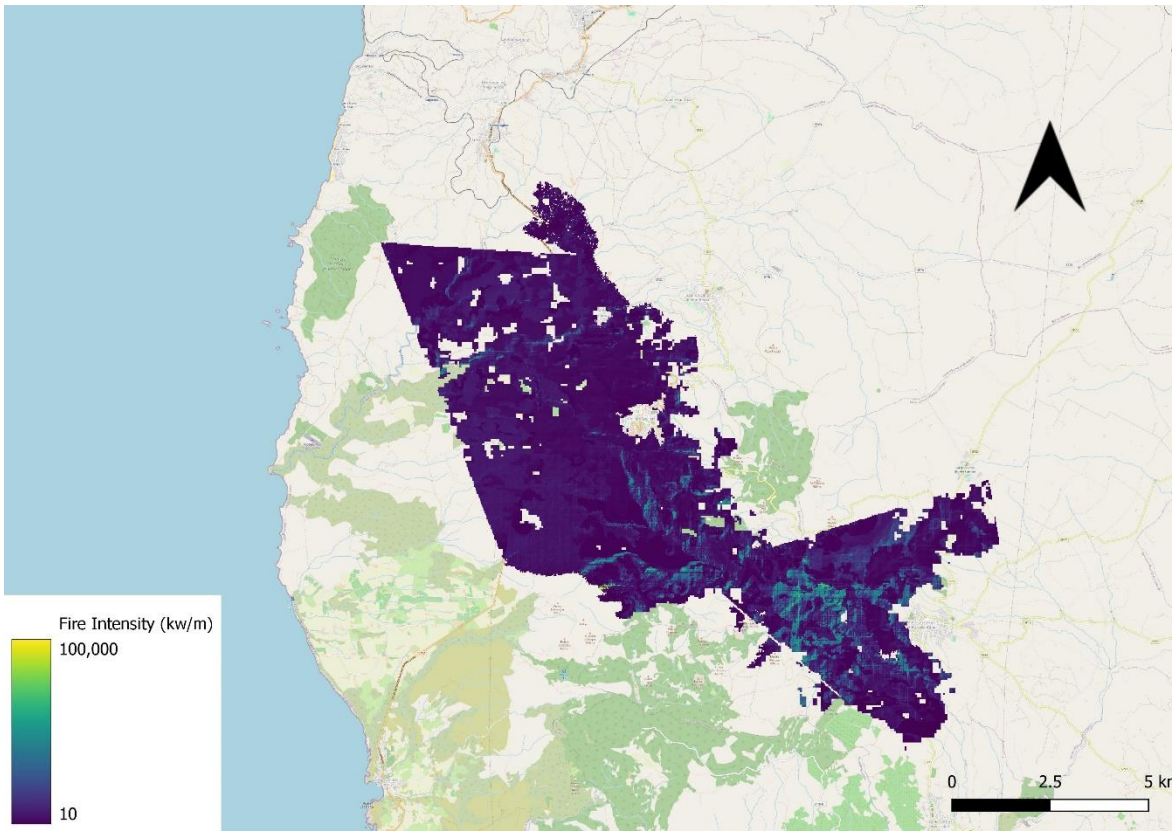

Figure 7.1.4 Result with modified vegetation and 15 lines (firefighting action)

E. Result with two phases (an ignition point + an ignition line) (Figure 7.1.5)

a)

- Ignition POINT: [40.119969;8.651672"] (DD)
- Wind speed: 45 – 30 [km/h]
- Wind direction: 135° - 235°
- Moisture content: 5 %
- Time limit: 60 min - 360 min

b)

- Ignition LINE: [[40.14858 40.13534]; [8.59120 8.53650]"] (DD)
- Wind speed: 30 – 45 - 30 [km/h]
- Wind direction: 155° - 180° - 235°
- Moisture content: 8 %
- Time limit: 60 min - 1200 min - 1800 min

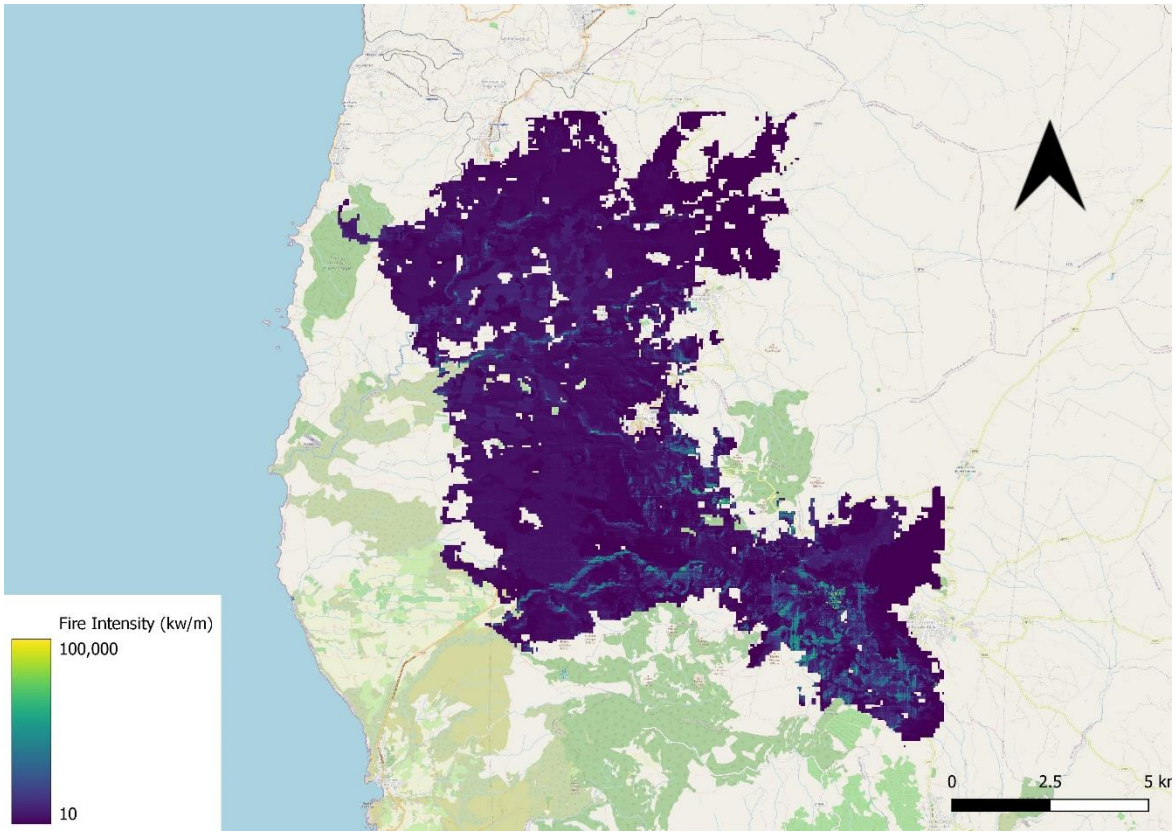

Figure 7.1.5 Result with two phases (an ignition point + an ignition line)

F. Result with arbitrary boundary conditions (Figure 7.1.6)

- Ignition point: [40°07'11.9"N 8°39'06.0"E (DMS), 40.119969, 8.651672(DD)]
- Wind speed: 40 – 60 [km/h]
- Wind direction: 135° - 145°
- Moisture content: 8 %
- Time limit: 780 min - 3600 min

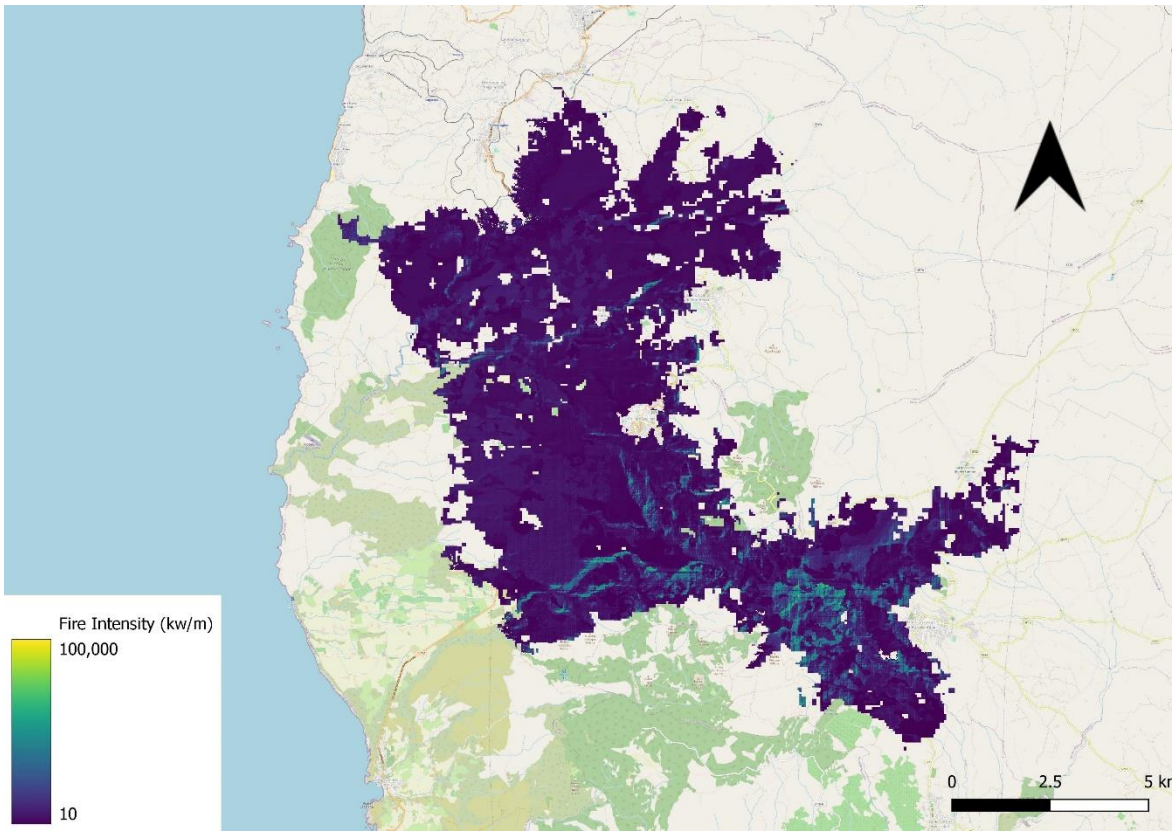

Figure 7.1.6 Result with arbitrary boundary conditions

7.2 Fire severity data

Google Earth Engine (GEE) is a powerful web platform for the cloud-based processing of remote sensing data on large scales. The advantage lies in its remarkable computation speed, as processing is outsourced to Google servers [54]. For the application of Burn Severity Mapping, there are two satellite data collections available: Landsat-8 and Sentinel-2. The user can choose from these two options. A brief overview of satellite data characteristics can be found below (Figure 7.2.1).

.

Satellite	**Landsat 8**	**Sentinel-2 (A&B)**
Launch date	February 11th, 2015	Jun 23rd,2015 & March 7th, 2017
Repetition rate	16 days	5 days (since 2017)
resolution	30 meters	10 meters
advantages	Longer time series Smaller export file	10 times higher spatial detail Higher chance of cloud-free images

Table 7.2.1 Characteristics of satellite data available for Burn Severity Mapping in GEE

Two periods for pre-fire and post-fire satellite images should be considered, following periods are used for our dNBR by Sentinel-2:

- For the time before the wildfire: '2021-06-15' -'2021-07-22'.
- For the time after the wildfire: '2021-07-28'- '2021-08-15'.

After calculating the dNBR map using GGE (Google Earth Engine) and categorizing it as explained above, the final severity map has been computed (Figure 7.2.1).

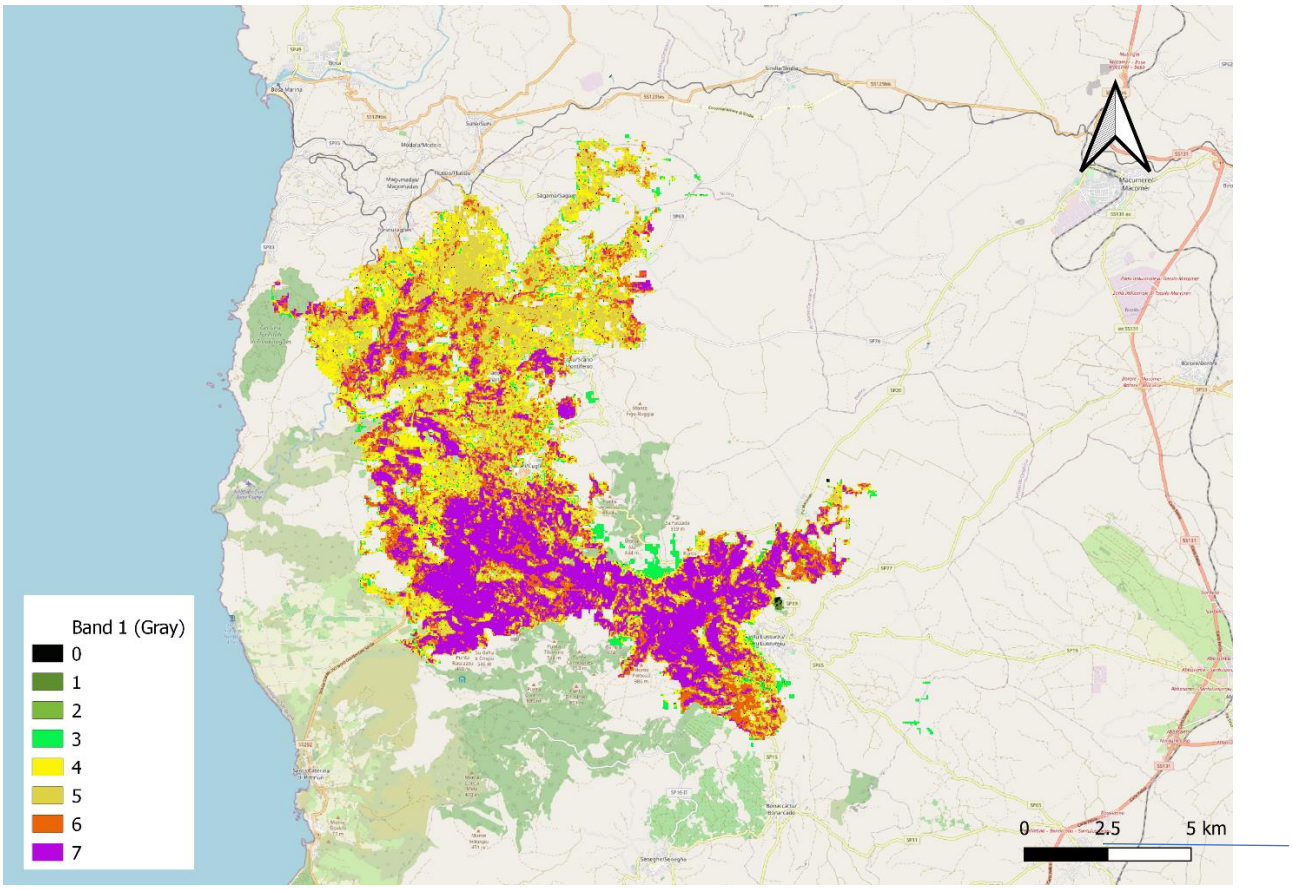

Figure 7.2.1 Using dNBR Sentinel-2 to estimate severity (Google earth engine)

7.3 Runoff results

First, the CRS (Coordinate Reference System) for the data used in the continuum is “EPSG:4326 WGS 84”, and the resolution is 0.005002 in degree. All pixels have been checked to be similar in terms of size, and numbers in rows and columns. Fire severity and the CN values map were overlapped to find the burn severity of each pixel. Different CN values of different areas have been modified using the three mentioned methods. To simplify calculations The Geopandas library in python was used. Figure 7.3.1 have demonstrated the fire severity of each pixel in the study area. The number of pixels also have illustrated in Table 7.3.1.

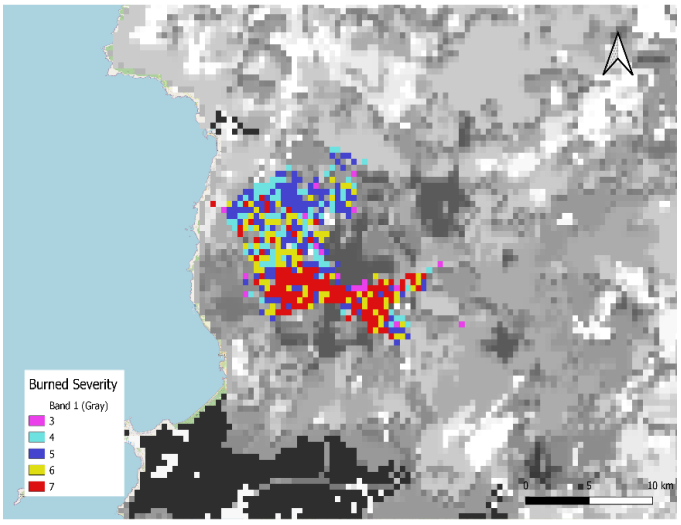

Figure 7.3.1 Pixels of each CN value burned with a specific level of severity

Number of pixels	Burn severity
168633	Not burned
188	low
173	Moderate-low
121	Moderate-high
139	high

Table 7.3.1 Number of pixels with different burn severity

The hydrologic soil group is another important characteristic of soil that will be considered in method number 3 in this study. Fuel characteristics play a key role in driving fire ignition and propagation.

Land cover along the coast and the main river valleys are dominated by sclerophyllous shrubs, thermos-Mediterranean Quercus ilex forests, and agricultural lands.

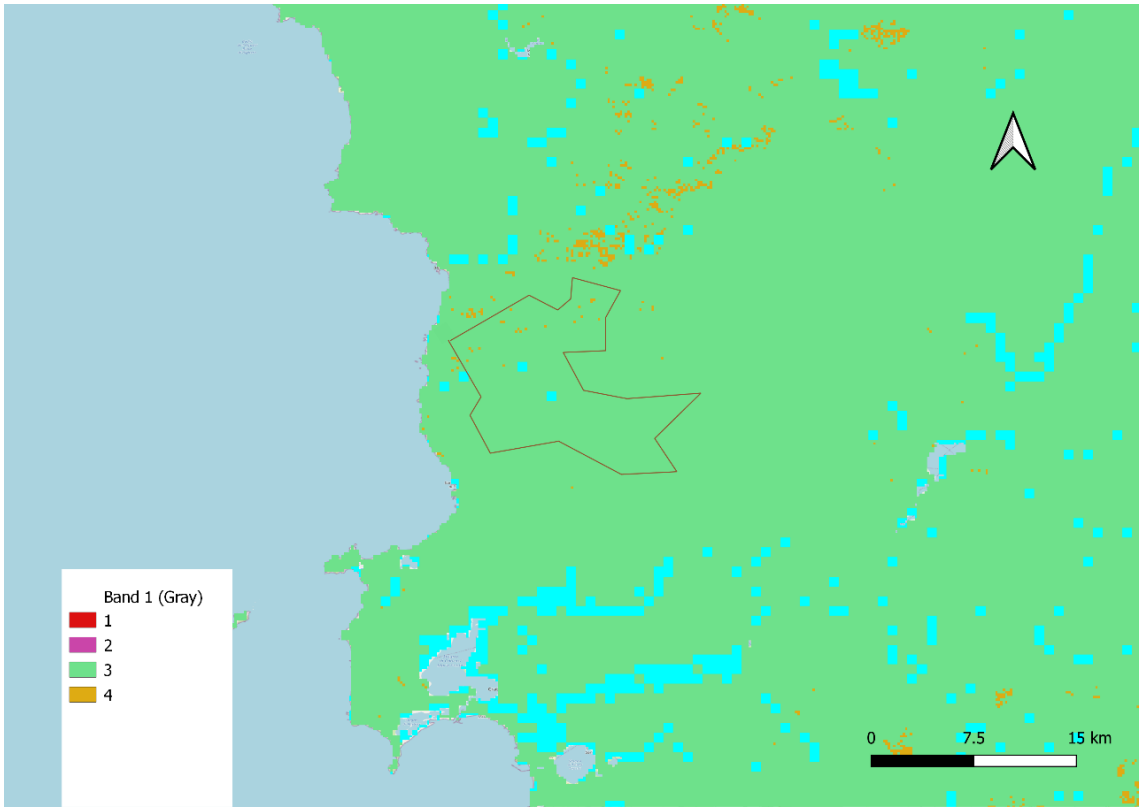

Figure 7.3.2 Hydrologic Soil Group (HSG)

According to Global Hydrologic Soil Groups for Curve Number-Based Runoff Modeling [55] (Figure 7.3.2), With an acceptable approximation, the soil group of type three is considered for whole the study area.

In terms of land cover and the vegetation type of the study area, the data from CORINE Land Cover 2018 [56] has been demonstrated below (Figure 7.3.3). The area is covered by the following landcover types:

- non-irrigated arable land [12]
- Olive groves [17]
- Pastures [18]
- Agro-forestry areas [22]
- Natural grasslands [26]
- Sclerophyllous vegetation [28]

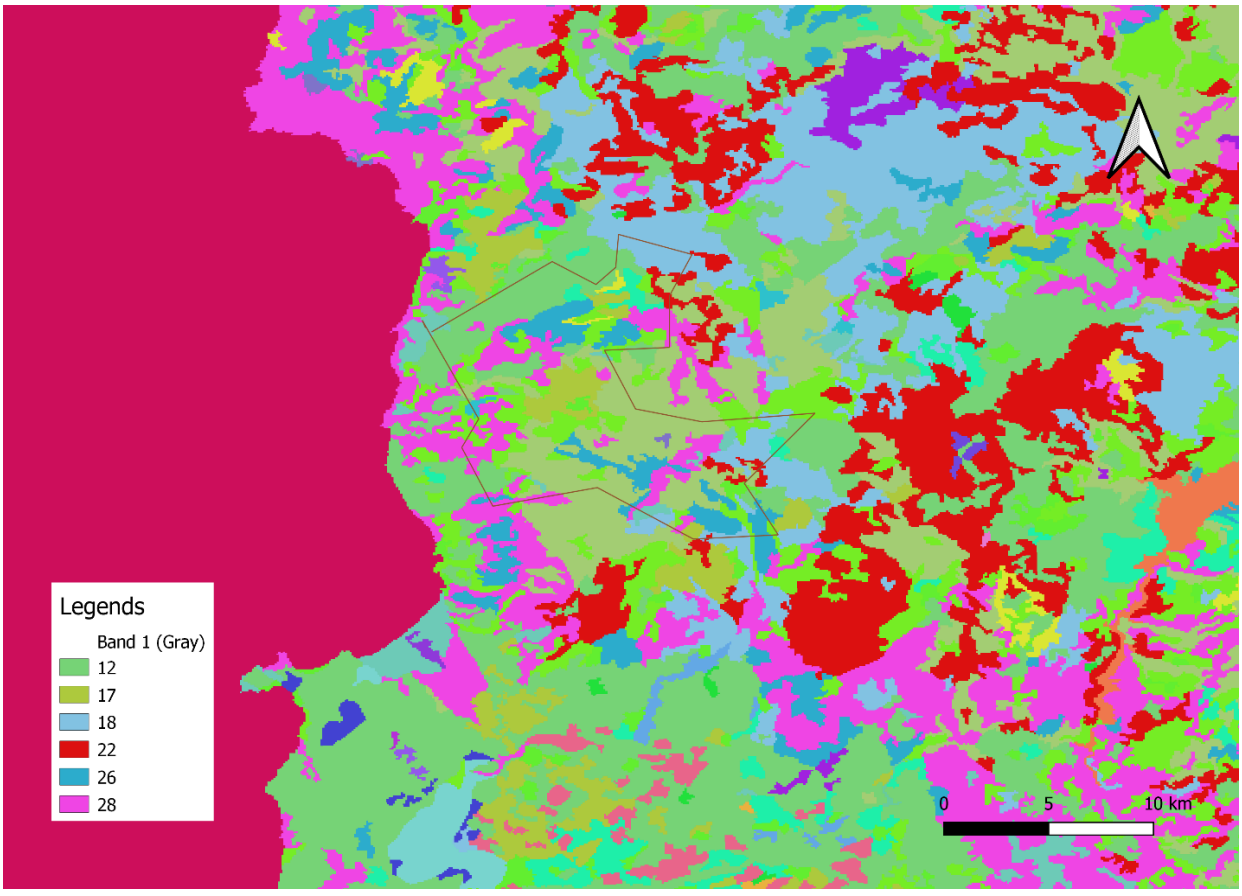

Figure 7.3.3 Landcover in the burned area

Figure 7.3.4 shows the codes which is written by python (in Jupyter IDE) for running the third method is present. The other two methods also used the same codes with changes in the parameters of new CN values.

3_Higginson and Jarnecke 2007

In [29]:
```
CN = gdal.Open(r"G:\LESSONS\Thesis\data for continuum\Initial\Rasters\CN_sardinia.tif")
CN_xyz = gdal.Translate(r"G:\LESSONS\Thesis\data for continuum\Initial\Rasters\CN_sardinia.xyz", CN)
CN_xyz =None
CN_csv = pd.read_csv(r"G:\LESSONS\Thesis\data for continuum\Initial\Rasters\CN_sardinia.xyz", sep = " ", header = None)
CN_csv.columns = ["x", "y", "CN"]
CN_csv.to_csv(r"G:\LESSONS\Thesis\data\Sardinia_cn_clipped.csv", index = False)
```

In [30]:
```
Fire_S = gdal.Open(r"G:\LESSONS\Thesis\data for continuum\Initial\Rasters\Fire_severity_Final.tif")
Fire_S_xyz = gdal.Translate(r"G:\LESSONS\Thesis\data for continuum\Initial\Rasters\Fire_severity_Final.xyz", Fire_S)
Fire_S_xyz =None
Fire_S3_csv = pd.read_csv(r"G:\LESSONS\Thesis\data for continuum\Initial\Rasters\Fire_severity_Final.xyz", sep = " ", header = No
Fire_S3_csv.columns = ["x", "y", "Fire Severity"]
Fire_S3_csv.to_csv(r"G:\LESSONS\Thesis\data for continuum\Initial\Rasters\Fire_severity_Final.csv", index = False)
```

In [31]:
```
fire_severity3 = Fire_S3_csv
cn3 = CN_csv

fire_severity3["CN"] = cn3["CN"]
```

In [32]:
```
fire_severity3
```

Out[32]:

	x	y	Fire Severity	CN
0	8.115001	41.276477	-9999	-9999.0
1	8.120003	41.276477	-9999	-9999.0
2	8.125005	41.276477	-9999	-9999.0
3	8.130007	41.276477	-9999	-9999.0

In [33]:
```
for i in range(0, fire_severity3.shape[0]):
    if fire_severity3["Fire Severity"][i] == 4:                    #Low
        fire_severity3["CN"][i] = fire_severity["CN"][i] + 5
    if fire_severity3["Fire Severity"][i] == 5:                    #moderate
        fire_severity3["CN"][i] = fire_severity["CN"][i] + 10
    if fire_severity3["Fire Severity"][i] == 6:                    #moderate
        fire_severity3["CN"][i] = fire_severity["CN"][i] + 10
    if fire_severity3["Fire Severity"][i] == 7:                    #high
        fire_severity3["CN"][i] = fire_severity["CN"][i] + 15
```

In [35]:
```
fire_severity3["CN"].max()
```

Out[35]: 108.0

In [36]:
```
for i in range(0, fire_severity3.shape[0]): # for replacing higher cn with 100
    if fire_severity3["CN"][i] > 100:
            fire_severity3["CN"][i] = 100
```

```
C:\Users\farzadazma\AppData\Local\Temp\ipykernel_596\2682297443.py:3: SettingWithCopyWarning:
A value is trying to be set on a copy of a slice from a DataFrame

See the caveats in the documentation: https://pandas.pydata.org/pandas-docs/stable/user_guide/indexing.html#returning-a-view-versus-a-copy
  fire_severity3["CN"][i] = 100
```

In [37]:
```
fire_severity3["CN"].max()
```

Out[37]: 100.0

In [38]:
```
fire_severity3.drop("Fire Severity", inplace=True, axis=1)
```

In [40]:
```
fire_severity3.to_csv(r"G:\LESSONS\Thesis\data for continuum\CN_post3_raster.xyz", index = False)
```

xyz to tif

In [41]:
```
CNraster = gdal.Translate(r"G:\LESSONS\Thesis\data for continuum\CN_method3.tif",
                          r"G:\LESSONS\Thesis\data for continuum\CN_post3_raster.xyz", outputSRS = "EPSG:4326")
CNraster = None
```

DONE

Figure 7.3.4 Python codes for Higginson and Jarnecke method

7.3.1 modified CN values

After using these methods to manipulate the CN values following CN maps for Sardinia were produced. All the resolutions and CRS (Coordinate Reference System) remained the same as the initial data. Results have illustrated in the following figures (Figure 7.3.5, Figure 7.3.6, Figure 7.3.7).

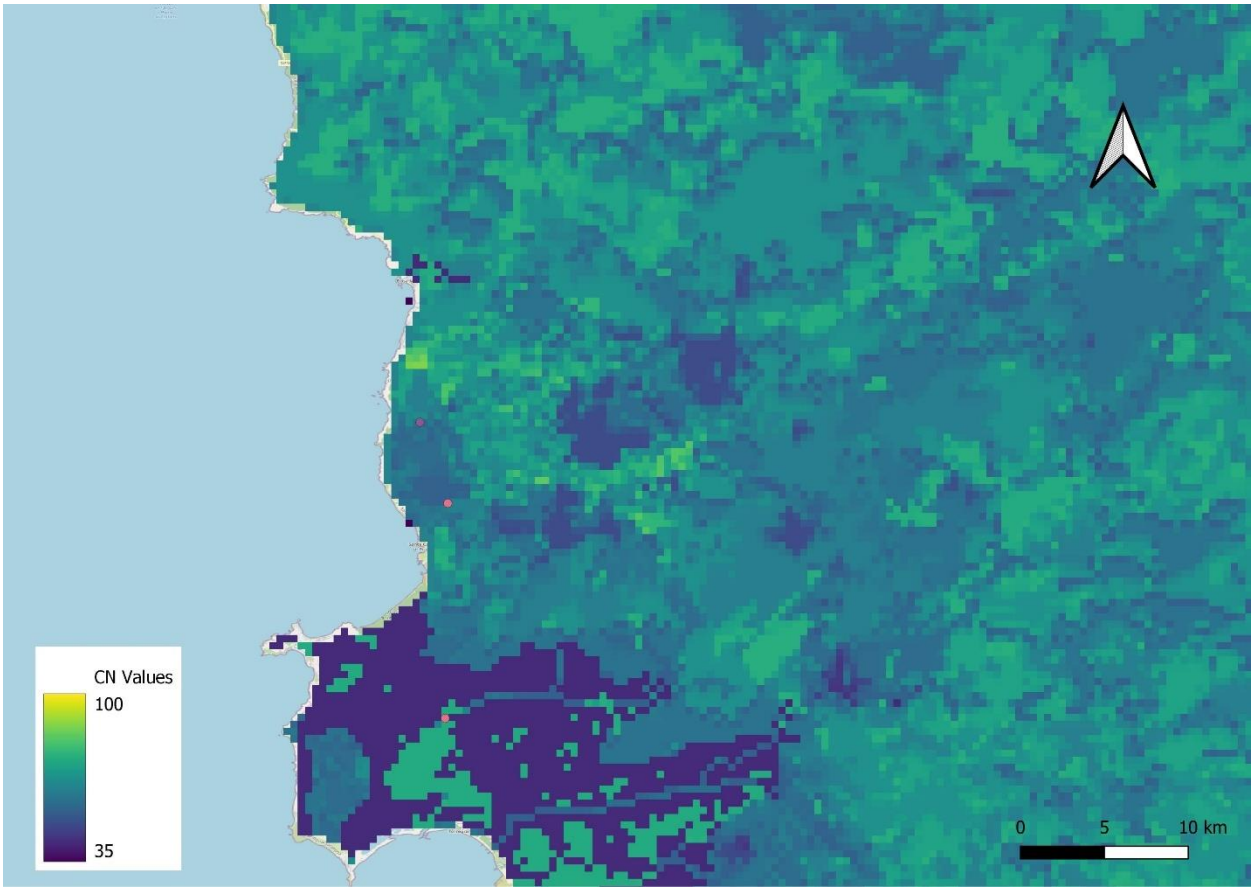

Figure 7.3.5 Modified CN values by Higginson and Jarnecke method

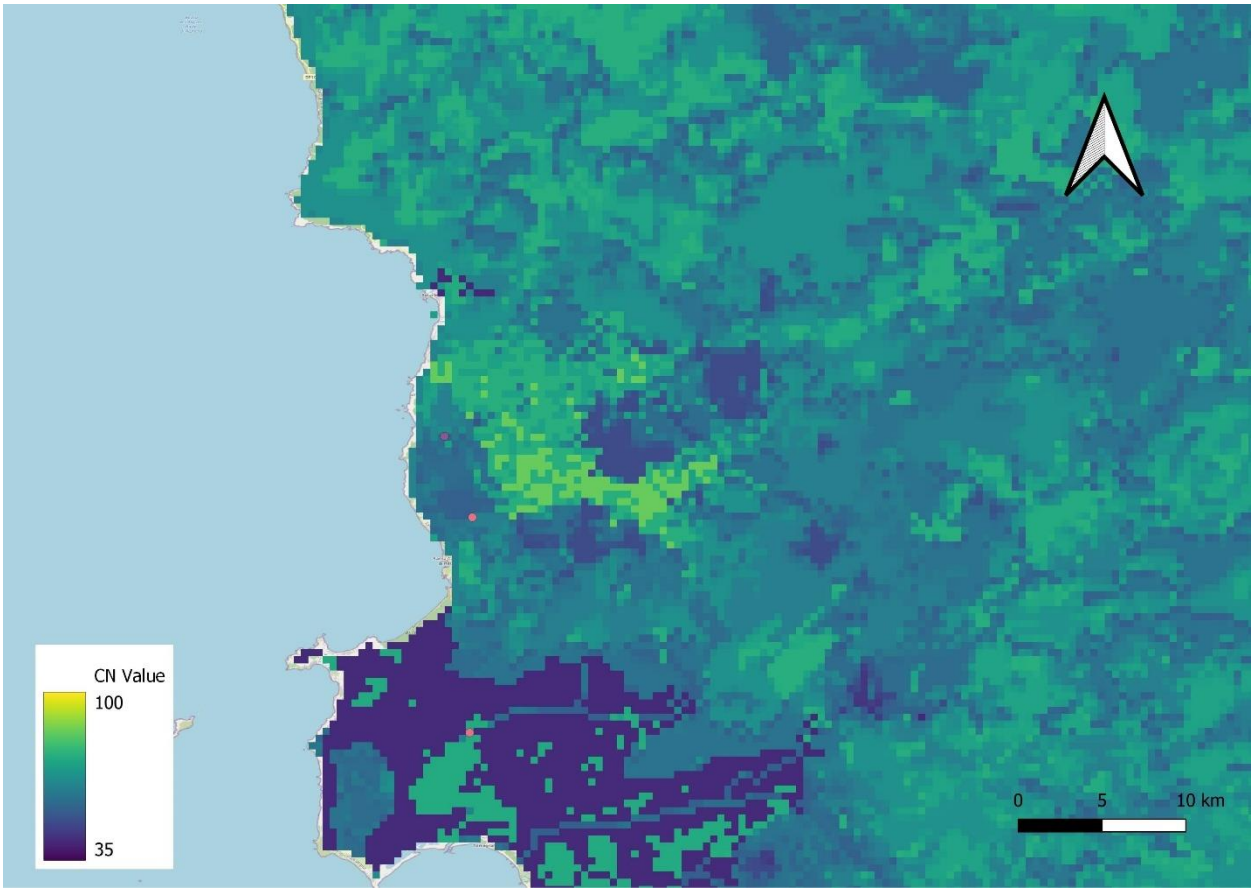

Figure 7.3.6 Modified CN values by Cerrelli method

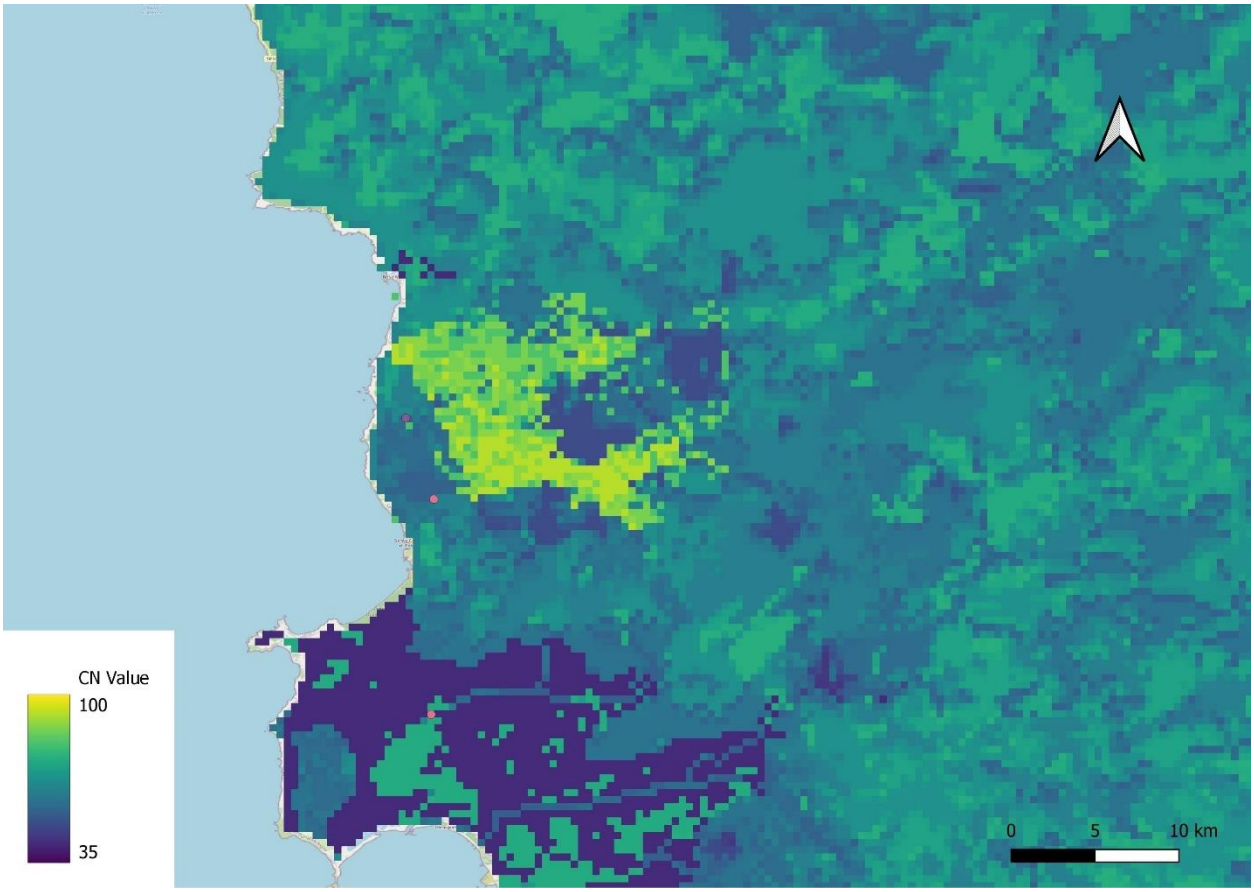

Figure 7.3.7 Modified CN values by Livingston method

8 DISCUSSION

8.1 To compare Fireline Intensity (results of PROPAGATOR) to fire severity (the result of dNBR)

This part is aimed to find a relation between Fireline Intensity (Figure 7.1.6 has been chosen due to having a better fit with fire severity) and fire severity (Figure 7.2.1) moreover topographical characteristics such as Dem, Aspect, and Slope with the behavior of the fire. The coordinate system for all the data (Fireline intensity raster from PROPAGATOR, fire severity from sentinel-2 data, DEM from Sardinia geoportale [57], aspect and slope which extracted from Dem by QGIS tools) should be the same, “EPSG:32632 WGS 84 / UTM zone 32N” coordinate reference system with the metric unit matched these data. Also, the extent of all rasters should be the same for having a DataFrame with a similar number of rows (pixels) (Figure 8.1.1).

"-9999" was signed to no value data and all no value data were removed from the DataFrame. Following DataFrame Is the result that was used to calculate of correlation:

	x	y	aspect	fire_intensity	slope	dem	fire_severity	clc
312870	460955	4457205	212.462524	3091.865234	5.482903	302.717590	5.0	73
312871	460965	4457205	199.708618	3726.549561	5.986861	303.080109	5.0	73
312872	460975	4457205	194.406998	3726.549561	6.314970	303.339386	5.0	73
312873	460985	4457205	193.407715	6461.759766	6.381196	303.598785	5.0	73
312874	460995	4457205	193.408829	6461.759766	6.381047	303.858093	5.0	73
...	...	...	...	...	...	...	...	...
3691135	469865	4440335	98.257065	3733.164307	9.725365	462.626709	3.0	70
3691136	469875	4440335	99.615425	3733.164307	9.318859	460.930695	3.0	86
3691137	469885	4440335	102.108482	4171.490234	8.378025	459.387695	3.0	86
3691138	469895	4440335	105.292664	4171.490234	7.849247	458.069489	3.0	86
3691139	469905	4440335	107.613037	3730.589355	7.905429	456.764313	3.0	86

1033169 rows × 8 columns

Figure 8.1.1 DataFrame for pixels of study area

Thanks to the Geospatial libraries (GDAL, RASTERIO, GEOPANDAS) of python all rasters were converted to one DataFrame with all the data for each pixel. Using the STATISTIC library, the Spearman and Pearson correlation was calculated for all features. The results are shown below (Figure 8.1.3 and Figure 8.1.2).

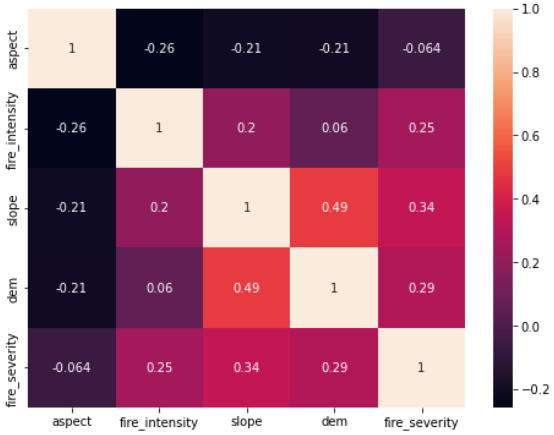

Figure 8.1.3 The Spearman rank correlation

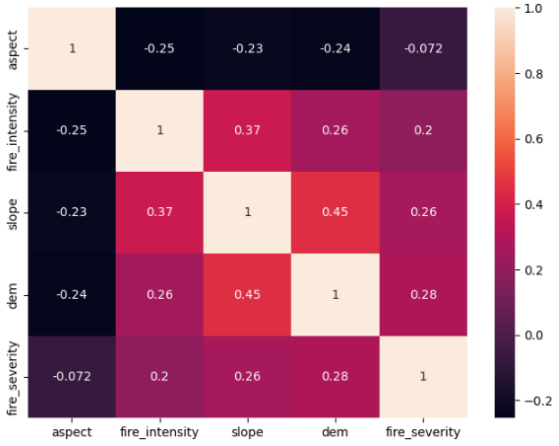

Figure 8.1.2 The Pearson correlation

According to figures, there is a positive relation between Fireline Intensity and fire severity. The slope has a negative relation to the number of fires. Surprisingly, this dataset shows that aspect does not correlate with the number of fires. The slope has a stronger relationship with Fireline Intensity rather than fire severity. Aspect has no contribution to the fire severity while a strong relationship with the Fireline Intensity. Fireline intensity cannot be used directly instead of fire severity in the considered method in this study.

8.2 Cascading effect of wildfire on CN value and consequently the runoff

Three basins which are affected by the fire are selected to evaluate the effects of wildfire. These basins names and other characteristics have demonstrated in Table 8.2.1.

Basin Names	Area (km^2)	Total burned area (km^2)	Burned Area (Km^2)			Burned Area (%)		
			Low Severity	Moderate Severity	High Severity	Low Severity	Moderate Severity	High Severity
Riu Mannu	156.87	64.884	14.894	36.983	13.007	9.5%	23.6%	8.3%
Riu Santa Caterina	231.29	17.282	2.132	6.556	8.594	0.9%	2.8%	3.7%
Pischilappiu a Riola Sardo	267.45	14.163	1.226	5.849	7.088	0.5%	2.2%	2.7%
Sum	655.62	96.33	18.25	49.39	28.69	10.9%	28.6%	14.7%

Table 8.2.1 Basins and their characteristics

Three points that have been chosen on these catchments are shown with their corresponding latitude longitude (Figure 8.2.1). These basins are respectively 156.870 km^2, 231.292 km^2, 267.454 km^2.

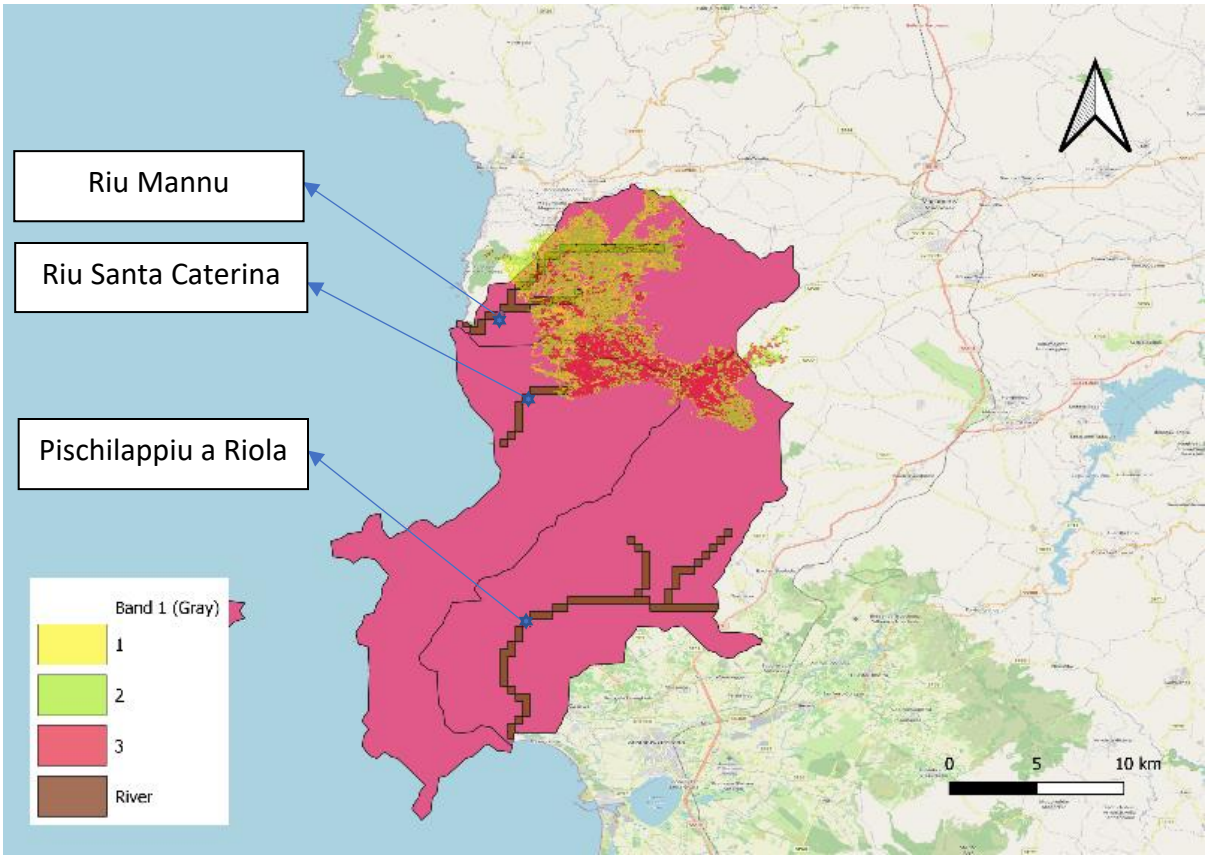

Figure 8.2.1 The location of rivers and basins with respect to the fire severity map (1- low severity, 2- moderate severity, 3- high severity)

- The first point on Riu Mannu: [40.1948805, 8.4946740] (DD)]
- The Second point on Riu Santa Caterina: [40.1340034, 8.5056925] (DD)]
- The Third point on Pischilappiu a Riola Sardo: [39.9923118, 8.5267639] (DD)]

These points have been used to extract the discharge (Q) data from our CONTINUUM results. Continuum is a distributed model based on a space-filling representation of the network, directly derived from a DEM. The DEM resolution coincides with the model resolution [14]. Dem which was used in this survey had a resolution of 0.005002 degrees. Data for running the continuum is the real data from 01-01-2017 to 01-01-2020. The time step to run the continuum for this data was 1 hour. It means 365 * 24* 3 discharges for each basin are provided.

The following figures (Figure 8.2.2 - Figure 8.2.13) illustrate discharge versus time at all three points for these three years. For each point, the first figure shows the discharges without considering the cascading (pre-fire) effect, then three methods are applied to obtain the rest of the figures(post-fire).

Original discharge- time (pre-fire) at Riu Mannu:

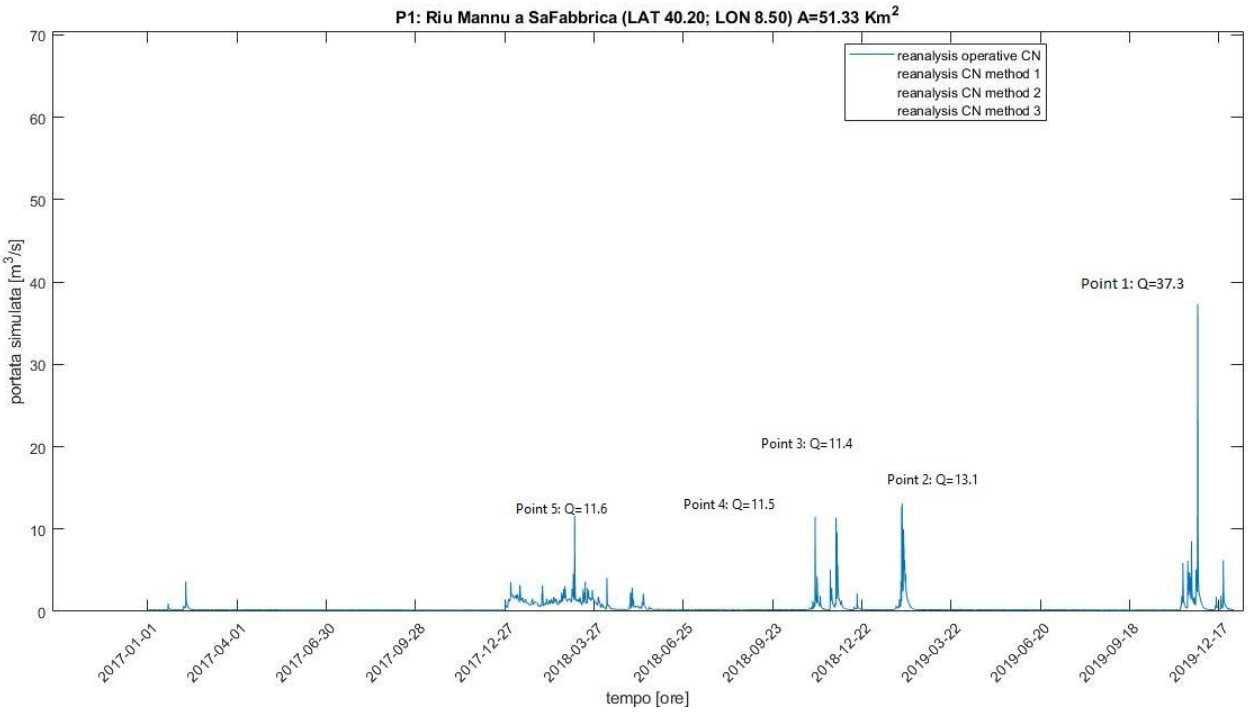

Figure 8.2.2 Discharges at the first point (on Riu Mannu a SaFabbrica) in original condition(pre-fire)

Discharge- time (post-fire) at Riu Mannu (using Livingston Method):

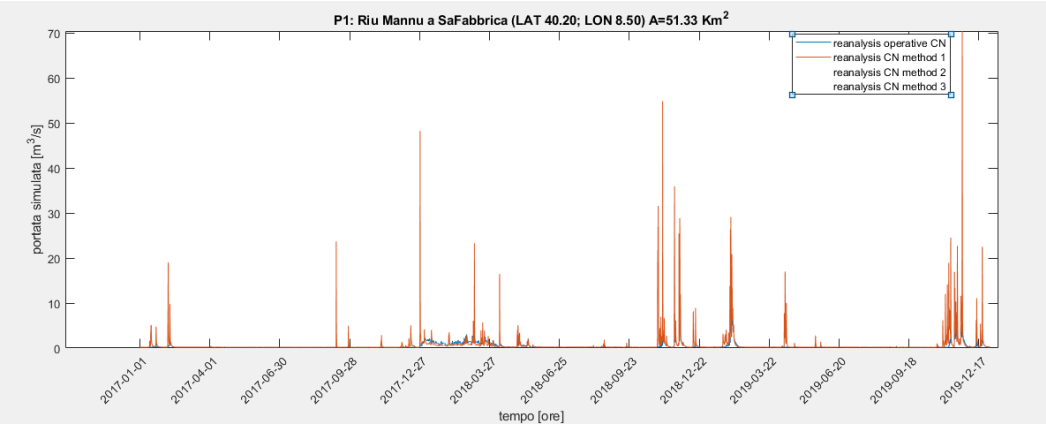

Figure 8.2.3 Discharges at the first point (on Riu Mannu a SaFabbrica) considering Livingston method

Discharge- time (post-fire) at Riu Mannu (using Cerrelli Method):

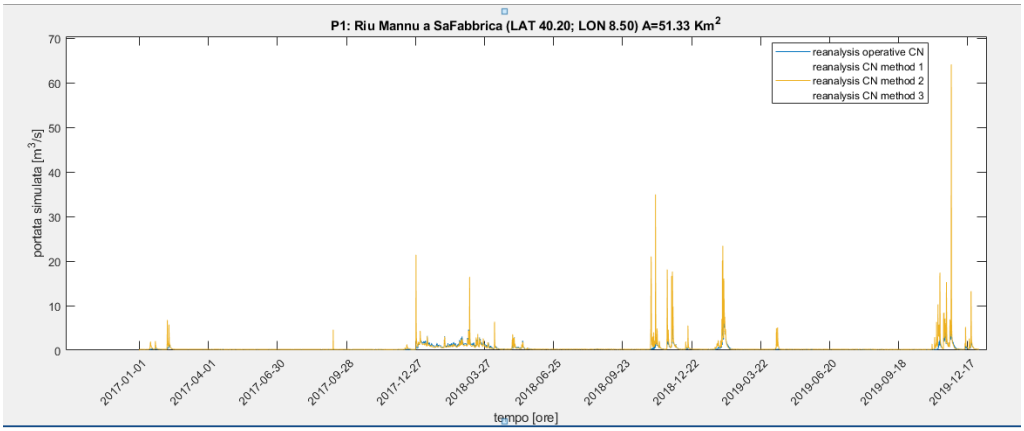

Figure 8.2.4 Discharges at the first point (on Riu Mannu a SaFabbrica) considering Cerrelli method

Discharge- time (post-fire) at Riu Mannu (using Higginson and Jarnecke Method):

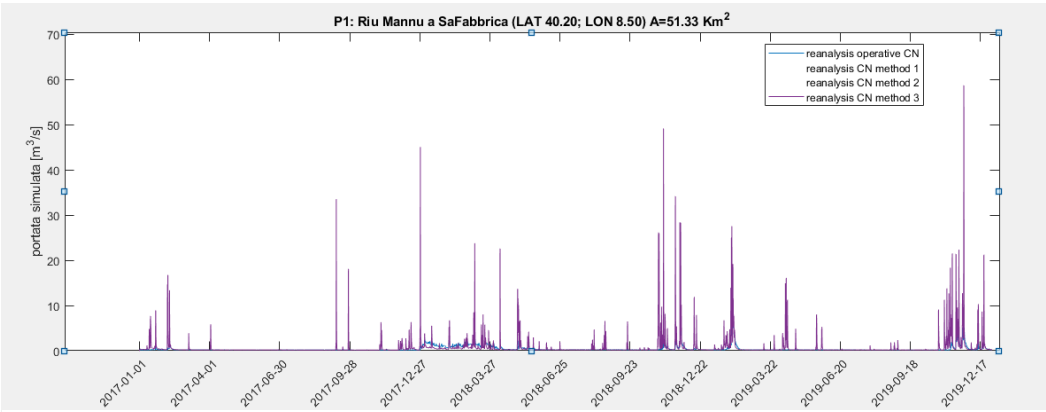

Figure 8.2.5 Discharges at the first point (on Riu Mannu a SaFabbrica) considering Higginson and Jarnecke method

Original discharge- time (pre-fire) at Riu Santa Caterina:

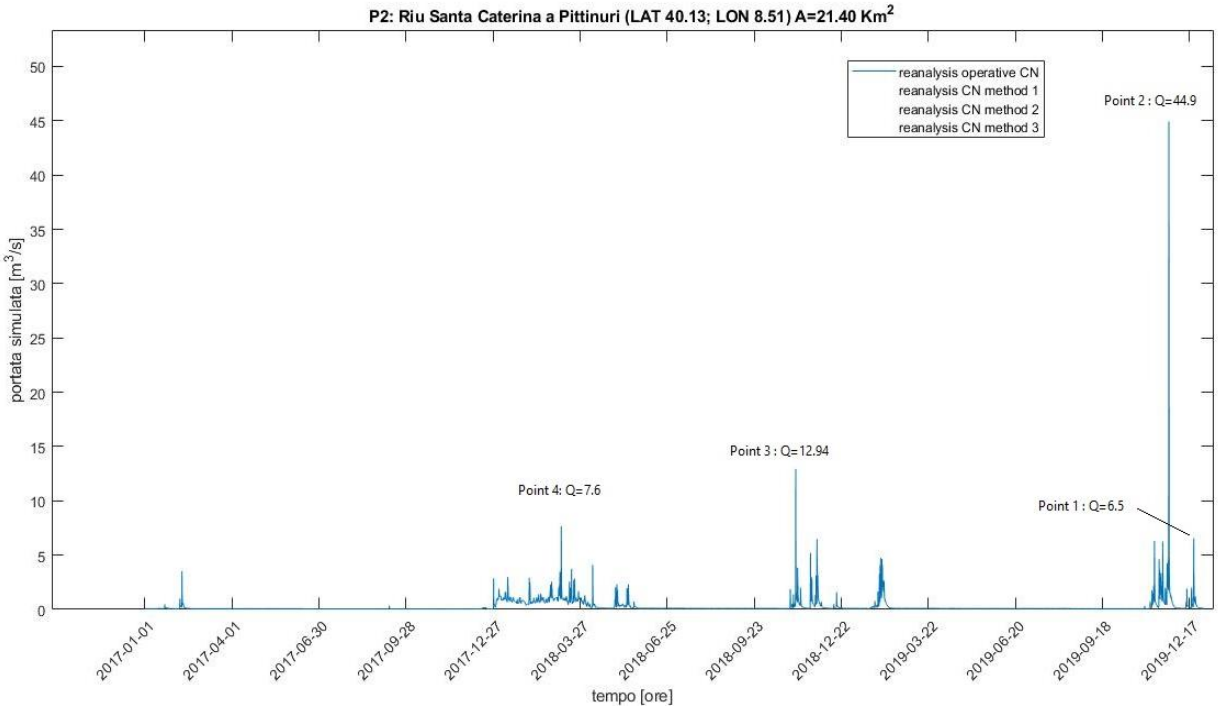

Figure 8.2.6 Discharges at the second point (on Riu Santa Caterina) in original condition(pre-fire)

Discharge- time (post-fire) at Riu Santa Caterina (using Livingston Method):

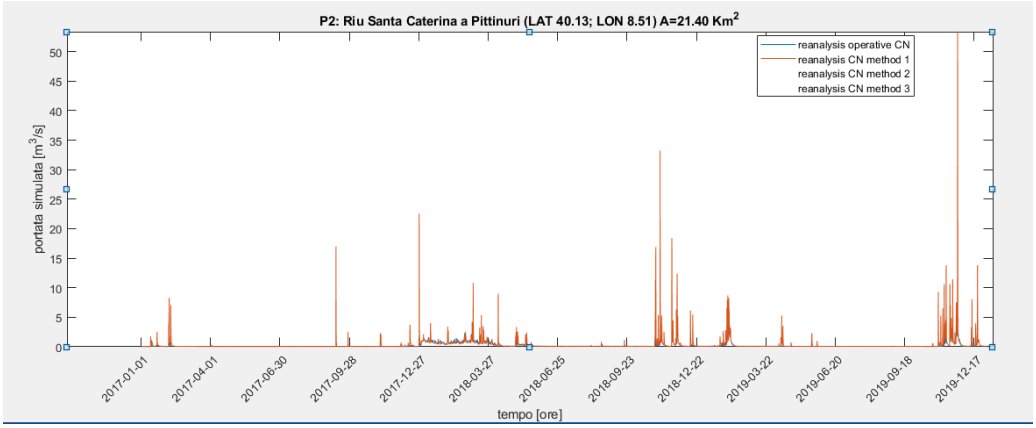

Figure 8.2.7 Discharges at the second point (on Riu Santa Caterina) considering Livingston method

Discharge- time (post-fire) at Riu Santa Caterina (using Cerrelli Method):

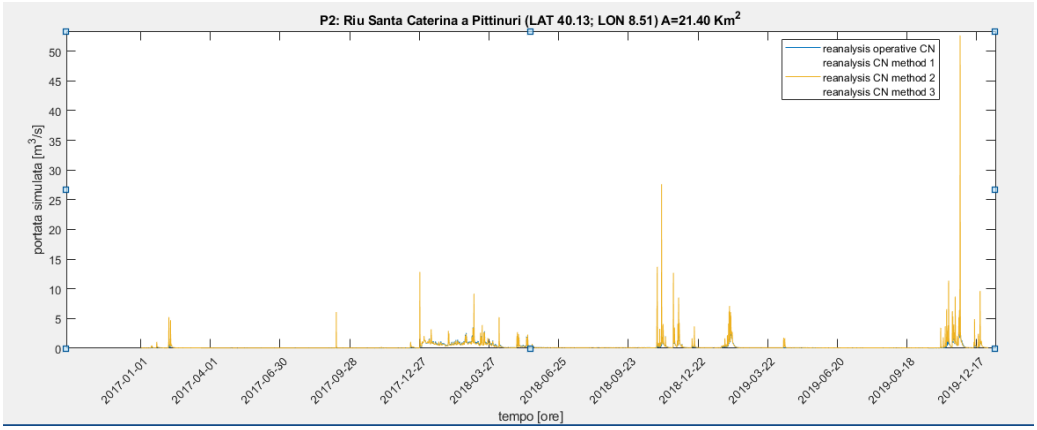

Figure 8.2.8 Discharges at the second point (on Riu Santa Caterina) considering Cerrelli method

Discharge- time (post-fire) at Riu Santa Caterina (using Higginson and Jarnecke Method):

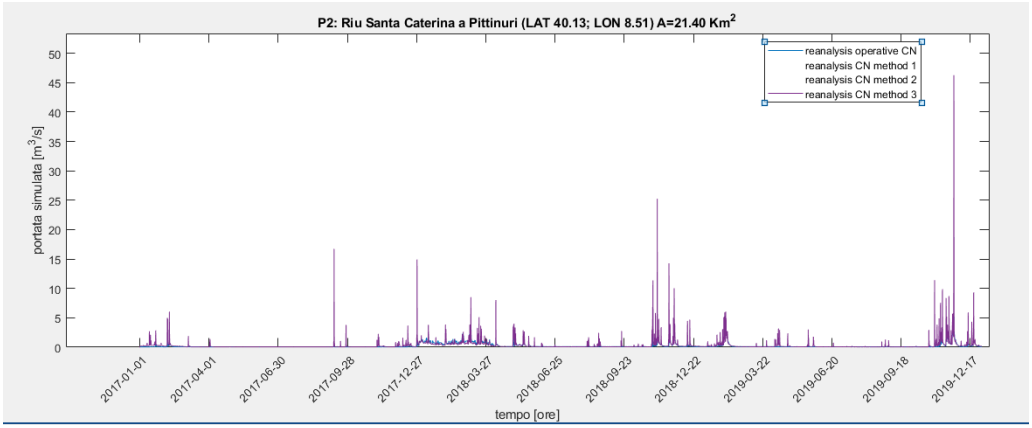

Figure 8.2.9 Discharges at the second point (on Riu Santa Caterina) considering Higginson and Jarnecke method

Original discharge- time (pre-fire) at Pischilappiu a Riola Sardo:

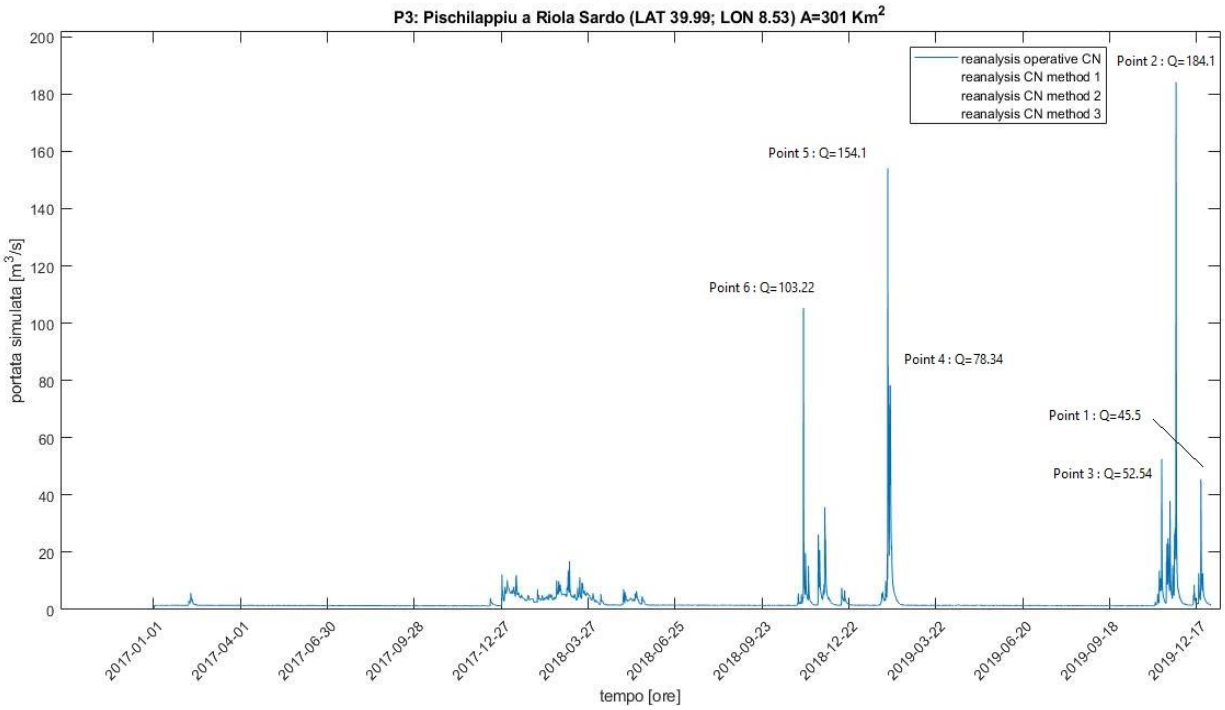

Figure 8.2.10 Discharges at the third point (on Pischilappiu a Riola Sardo) in original condition(pre-fire)

Discharge- time (post-fire) at Pischilappiu a Riola Sardo (using Livingston Method):

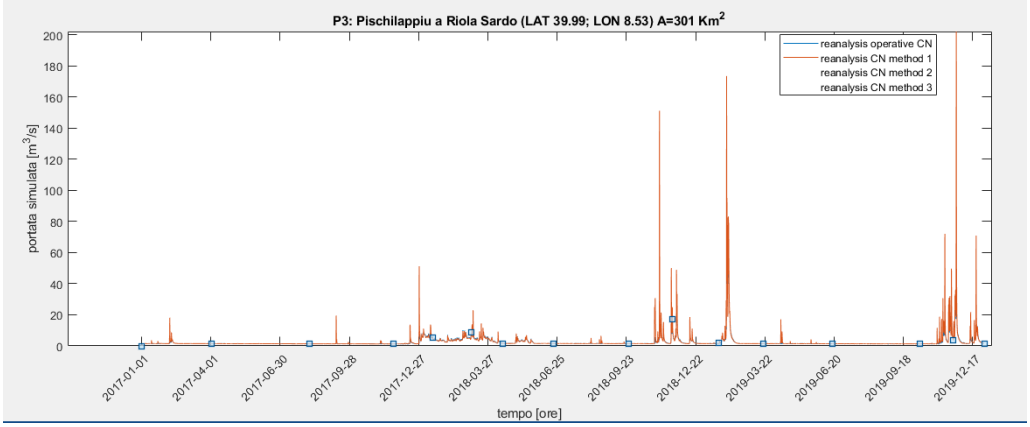

Figure 8.2.11 Discharges at the third point (on Pischilappiu a Riola Sardo) considering Livingston method

Discharge- time (post-fire) at Pischilappiu a Riola Sardo (using Cerrelli Method):

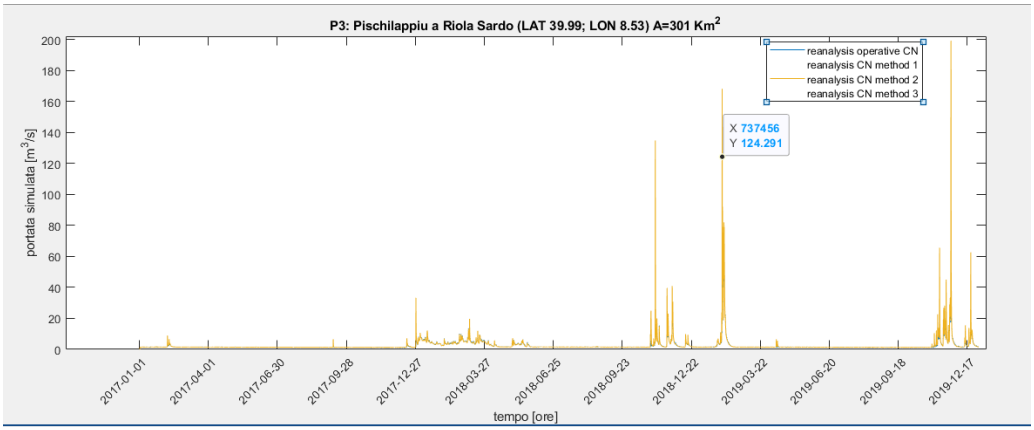

Figure 8.2.12 Discharge at the third point (Pischilappiu a Riola Sardo) considering Cerrelli method

Discharge- time (post-fire) at Pischilappiu a Riola Sardo (using Higginson and Jarnecke Method):

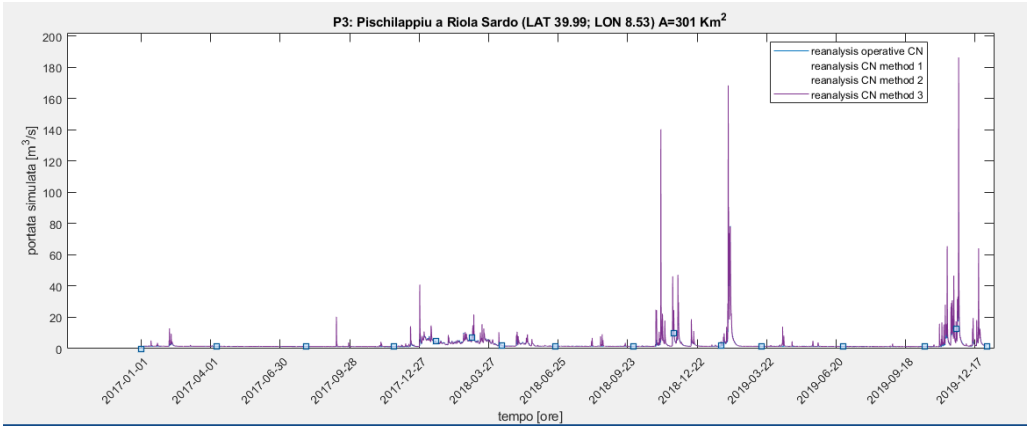

Figure 8.2.13 Discharges at the third point (on Pischilappiu a Riola Sardo) considering Higginson and Jarnecke method

The result of the graphs and the hourly discharge simulation by the CONTINUUM have been summarized in the charts below. According to the graphs, the main Maximum discharges and corresponding changes were selected and have been shown below (Table 8.2.2 and Table 8.2.3). These points are mentioned on graphs in each initial discharge of basins.

Extreme discharges	Riu Mannu				Riu Santa Caterina				Pischilappiu a Riola Sardo			
	Q_0*	Q_1*	Q_2*	Q_3*	Q_0	Q_1	Q_2	Q_3	Q_0	Q_1	Q_2	Q_3
1	37.3	70.5	64.2	58.7	44.9	53.4	52.6	46.3	184.1	202.0	199.2	186.3
2	13.1	41.4	27.7	37.4	12.9	26.8	23.9	21.9	154.1	162.2	161.2	167.0
3	11.6	35.7	21.9	32.1	7.7	18.3	12.8	14.3	103.2	123.0	115.4	114.1
4	11.5	35.7	21.4	31.6	6.5	16.8	11.4	12.2	78.3	88.2	85.6	84.1
5	11.4	31.6	21.4	31.5	-	-	-	-	52.5	59.7	57.4	56.8
6	-	-	-	-	-	-	-	-	45.5	51.2	49.6	49.6

Table 8.2.2 Changes for Max discharges for each basin based on each method

Extreme discharges	Riu Mannu			Riu Santa Caterina			Pischilappiu a Riola Sardo		
	Q_1	Q_2	Q_3	Q_1	Q_2	Q_3	Q_1	Q_2	Q_3
1	88.8%	71.9%	57.3%	18.7%	17.1%	3.0%	9.7%	8.2%	1.2%
2	216.1%	111.2%	185.5%	106.9%	84.9%	69.3%	5.3%	4.6%	8.4%
3	208.0%	88.6%	177.1%	139.4%	67.8%	86.5%	19.2%	11.8%	10.5%
4	211.6%	86.8%	175.9%	159.0%	75.2%	87.6%	12.7%	9.3%	7.4%
5	178.0%	88.3%	176.8%	-	-	-	13.7%	9.2%	8.1%
6	-	-	-	-	-	-	12.5%	8.9%	8.9%

Table 8.2.3 Changes for Max discharges for each basin based on each method (Percentages)

* Q_0 = Initial discharges
* Q_1 = Discharge resulting from Livingston method
* Q_2 = Discharge resulting from Cerrelli method
* Q_3 = Discharge resulting from Higginson and Jarnecke method

9 DISCUSSION AND CONCLUSION

As indicated in the previous part of the thesis three methods have been considered for the runoff estimation after the wildfire in three adjacent basins (Riu Mannu, Riu Santa Caterina, and Pischilappiu) affected by a severe fire in Sardinia. First, let us consider the Number of significant events based on the maximum discharge of each basin during the three years. The result illustrates significant growth in the number of events after modification of the CN values based on the three mentioned method. Depending on basins, methods and surprisingly on the volume of the discharge, there was a diverse enhancement in simulated discharges.

In the Riu Mannu catchment where the upstream area has been affected mostly (36.98 km^2 of the basin) by moderate severity and partly by low and high severity (respectively 14.89 km^2 and 13 km^2) severity, the number of significant discharges had been doubled on average. In terms of discharge values, Livingston method shows a higher increase (on an average of 180%) than Higginson and Jarnecke method (an average of 154%), and the lowest changes belong to Cerrelli method (an average of 90%).

In the Riu Santa Caterina basin than 6.57 km^2 of the upstream area was affected by moderate severity, 8.6 km^2 with high severity, and 2.13 km^2 with low severity. The data shows around 40% growth for the number of significant events for this basin. Discharges have increased by about 100% for the Livingston method and around 60% for the two other methods.

In the last case, Pischilappiu catchment that the upstream area was affected by high and moderate severity individually with 7.9 km^2 and 5.85 km^2, in terms of number of significant events, the data shows lower enhancement around 15%. Considering discharge values, Livingston method has 12% higher discharges, while Cerrelli and Higginson and Jarnecke methods show 8% growth.

The summary of the number of events and number of peaks in the discharge-time plot, based on results coming from CONTINUUM, has been shown below (Table 8.2.4).

-	Basin	Pre-fire	Livingston Method	Cerrelli Method	Higginson and Jarnecke Method
Number of events above half of the max discharge of each Basin*	**Riu Mannu**	6	18	9	22
	Riu Santa Caterina	5	8	6	7
	Pischilappiu a Riola Sardo	15	18	17	18
Increasement in %	**Riu Mannu**	-	200.0%	50.0%	266.7%
	Riu Santa Caterina	-	60.0%	20.0%	40.0%
	Pischilappiu a Riola Sardo	-	20.0%	13.3%	20.0%

‘

Table 8.2.4 The summary of the Continuum results

* The significant discharges have been described as the discharges that are higher than half of maximum discharge (equation below) in each basin individually.

$$Q > \frac{\text{maximum discharge for each basin}}{2}$$

As the rain input used by the model is a product of gauges and radar merging, the results vary due to several reasons, different fire severity in the region, different new CN values produced by each method, the difference in location of the affected area by the fire with respect to the upstream of selected points on the rivers.

Fire severity from EO (Earth Observation) is not fully representative of the Fireline intensity, does not considering the type of vegetation burned, reducing the capacity to evaluate the impact on the soil structure and the recovery time after the fire. However, the availability of propagation models able to simulate the Fireline intensity and can represent a suitable opportunity for the evaluation of the impact of the fire on the soil properties.

The lack of field data in burned catchments and related research to verify the effect on CN hampers post-fire runoff modeling with CNs. There is little research adequate to determine best-fit runoff CNs, even for unburned mountain and forested watersheds. The variability of the discharge using three different methods is significant producing very high uncertainty.

In conclusion, it is evident that there is still large room for improving the capacity to predict cascading effects combining different simulation tools. In general, there is a need to have more in field data also by the support of the UAV (Unmanned aerial vehicle).

10 REFERENCES

[1] D. M. J. S. Bowman et al., “Fire in the Earth System.” [Online]. Available: https://www.science.org

[2] K. Pavlek et al., “Spatial patterns and drivers of fire occurrence in a Mediterranean environment: a case study of southern Croatia,” Geografisk Tidsskrift - Danish Journal of Geography , vol. 117, no. 1, pp. 22–35, Jan. 2017, doi: 10.1080/00167223.2016.1266272.

[3] “Annual_Report_2021_EFFIS”.

[4] U. States Department of Agriculture and N. Resources Conservation Service, “Hydrologic Analyses of Post-Wildfire Conditions Natural Resources Conservation Service,” 2016. [Online]. Available: http://www.ocio.usda.gov/sites/

[5] J. A. Moody, D. A. Martin, S. L. Haire, and D. A. Kinner, “Linking runoff response to burn severity after a wildfire,” Hydrol Process, vol. 22, no. 13, pp. 2063–2074, Jun. 2008, doi: 10.1002/hyp.6806.

[6] M. Salis et al., “Application of simulation modeling for wildfire exposure and transmission assessment in Sardinia, Italy,” International Journal of Disaster Risk Reduction, vol. 58, May 2021, doi: 10.1016/j.ijdrr.2021.102189.

[7] B. A. Ebel, J. A. Moody, and D. A. Martin, “Post-fire temporal trends in soil-physical and -hydraulic properties and simulated runoff generation: Insights from different burn severities in the 2013 Black Forest Fire, CO, USA,” Science of the Total Environment, vol. 802, Jan. 2022, doi: 10.1016/j.scitotenv.2021.149847.

[8] G. A. Cerrelli, “FIRE HYDRO, A Simplified Method for Predicting Peak Discharges to Assist in the Design of Flood Protection Measures for Western Wildfires,” 2005.

[9] K. X. Soulis, “Estimation of SCS Curve Number variation following forest fires,” Hydrological Sciences Journal, vol. 63, no. 9, pp. 1332–1346, Jul. 2018, doi: 10.1080/02626667.2018.1501482.

[10] R. SHAKESBY and S. DOERR, “Wildfire as a hydrological and geomorphological agent,” Earth Sci Rev, vol. 74, no. 3–4, pp. 269–307, Feb. 2006, doi: 10.1016/j.earscirev.2005.10.006.

[11] M. Conedera, L. Peter, P. Marxer, F. Forster, D. Rickenmann, and L. Re, “Consequences of forest fires on the hydrogeological response of mountain catchments: a case study of the Riale Buffaga, Ticino, Switzerland,” Earth Surf Process Landf, vol. 28, no. 2, pp. 117–129, Feb. 2003, doi: 10.1002/esp.425.

[12] “CIMA Foundation - Continuum.” https://www.cimafoundation.org/fondazioni/ricerca-sviluppo/continuum.html (accessed Nov. 08, 2022).

[13] “CIMA Research Foundation - Propagator.” https://www.cimafoundation.org/foundations/research-development/propagator.html (accessed Nov. 08, 2022).

[14] F. Silvestro, S. Gabellani, F. Delogu, R. Rudari, and G. Boni, “Exploiting remote sensing land surface temperature in distributed hydrological modelling: The example of the Continuum model,” Hydrol Earth Syst Sci, vol. 17, no. 1, pp. 39–62, 2013, doi: 10.5194/hess-17-39-2013.

[15] M. Kemter et al., “Cascading Hazards in the Aftermath of Australia’s 2019/2020 Black Summer Wildfires,” Earth’s Future, vol. 9, no. 3. John Wiley and Sons Inc, Mar. 01, 2021. doi: 10.1029/2020EF001884.

[16] R. A. Shakesby and S. H. Doerr, “Wildfire as a hydrological and geomorphological agent,” Earth Sci Rev, vol. 74, no. 3–4, pp. 269–307, Feb. 2006, doi: 10.1016/j.earscirev.2005.10.006.

[17] J. A. Vega, C. Fernández, and T. Fonturbel, “Throughfall, runoff and soil erosion after prescribed burning in gorse shrubland in Galicia (NW Spain),” Land Degrad Dev, vol. 16, no. 1, pp. 37–51, Jan. 2005, doi: 10.1002/ldr.643.

[18] M. de Luis, J. C. González-Hidalgo, and J. Raventós, “Effects of fire and torrential rainfall on erosion in a Mediterranean gorse community,” Land Degrad Dev, vol. 14, no. 2, pp. 203–213, Mar. 2003, doi: 10.1002/ldr.547.

[19] E. Marcos, R. Tarrega, and E. Luis-Calabuig, “Comparative Analysis of Runo and Sediment Yield with a Rainfall Simulator After Experimental Fire,” Arid Soil Research and Rehabilitation, vol. 14, no. 3, pp. 293–307, Jan. 2000, doi: 10.1080/089030600406699.

[20] A. Cerdà, “Changes in overland flow and infiltration after a rangeland fire in a Mediterranean scrubland,” Hydrol Process, vol. 12, no. 7, pp. 1031–1042, Jun. 1998, doi: 10.1002/(SICI)1099-1085(19980615)12:7<1031::AID-HYP636>3.0.CO;2-V.

[21] A. G. Mayor, S. Bautista, J. Llovet, and J. Bellot, “Post-fire hydrological and erosional responses of a Mediterranean landscpe: Seven years of catchment-scale dynamics,” Catena (Amst), vol. 71, no. 1, pp. 68–75, Sep. 2007, doi: 10.1016/j.catena.2006.10.006.

[22] A. G. Mayor, S. Bautista, J. Llovet, and J. Bellot, “Post-fire hydrological and erosional responses of a Mediterranean landscpe: Seven years of catchment-scale dynamics,” Catena (Amst), vol. 71, no. 1, pp. 68–75, Sep. 2007, doi: 10.1016/j.catena.2006.10.006.

[23] M. A. Marque´s and E. Mora, “The influence of aspect on runoff and soil loss in a Mediterranean burnt forest (Spain),” Catena (Amst), vol. 19, no. 3–4, pp. 333–344, Jun. 1992, doi: 10.1016/0341-8162(92)90007-X.

[24] M. Salis et al., “Assessing exposure of human and ecological values to wildfire in Sardinia, Italy,” Int J Wildland Fire, vol. 22, no. 4, pp. 549–565, 2013, doi: 10.1071/WF11060.

[25] A. M. Kinoshita, T. S. Hogue, and C. Napper, “Evaluating Pre- and Post-Fire Peak Discharge Predictions across Western U.S. Watersheds,” J Am Water Resour Assoc, vol. 50, no. 6, pp. 1540–1557, Dec. 2014, doi: 10.1111/jawr.12226.

[26] R. K. Livingston, T. A. Earles, and K. R. Wright, “Los Alamos Post-Fire Watershed Recovery: A Curve-Number-Based Evaluation,” in Managing Watersheds for Human and Natural Impacts, Jul. 2005, pp. 1–11. doi: 10.1061/40763(178)41.

[27] B. M. Q. Ong and F. P. Cacciafoco, “Unveiling the Enigmatic Origins of Sardinian Toponyms,” Languages, vol. 7, no. 2, Jun. 2022, doi: 10.3390/LANGUAGES7020131.

[28] “SardegnaTurismo - Sito ufficiale del turismo della Regione Sardegna.” https://www.sardegnaturismo.it/ (accessed Oct. 27, 2022).

[29] “Italy: Evacuations and disruptions in Oristano area of Sardinia due to wildfire, July 25 | Crisis24.” https://crisis24.garda.com/alerts/2021/07/italy-evacuations-and-disruptions-in-oristano-area-of-sardinia-due-to-wildfire-july-25 (accessed Oct. 27, 2022).

[30] J. E. Keeley, “Fire intensity, fire severity and burn severity: A brief review and suggested usage,” Int J Wildland Fire, vol. 18, no. 1, pp. 116–126, 2009, doi: 10.1071/WF07049.

[31] S. Gabellani, F. Silvestro, R. Rudari, and G. Boni, “General calibration methodology for a combined Horton-SCS infiltration scheme in flash flood modeling,” 2008. [Online]. Available: www.nat-hazards-earth-syst-sci.net/8/1317/2008/

[32] G. Esposito et al., “Characterizing consecutive flooding events after the 2017 Mt. Salto Wildfires (Southern Italy): Hazard and emergency management implications,” Water (Switzerland), vol. 11, no. 12, Dec. 2019, doi: 10.3390/W11122663.

[33] F. Carvajal-Ramírez, J. R. Marques da Silva, F. Agüera-Vega, P. Martínez-Carricondo, J. Serrano, and F. J. Moral, “Evaluation of Fire Severity Indices Based on Pre- and Post-Fire Multispectral Imagery Sensed from UAV,” Remote Sens (Basel), vol. 11, no. 9, p. 993, Apr. 2019, doi: 10.3390/rs11090993.

[34] G. Mallinis, I. Mitsopoulos, and I. Chrysafi, “Evaluating and comparing Sentinel 2A and Landsat-8 Operational Land Imager (OLI) spectral indices for estimating fire severity in a Mediterranean pine ecosystem of Greece,” GIsci Remote Sens, vol. 55, no. 1, pp. 1–18, Jan. 2018, doi: 10.1080/15481603.2017.1354803.

[35] L. B. Lentile et al., “Remote sensing techniques to assess active fire characteristics and post-fire effects,” Int J Wildland Fire, vol. 15, no. 3, p. 319, 2006, doi: 10.1071/WF05097.

[36] G. Mallinis, I. Mitsopoulos, and I. Chrysafi, “Evaluating and comparing Sentinel 2A and Landsat-8 Operational Land Imager (OLI) spectral indices for estimating fire severity in a Mediterranean pine ecosystem of Greece,” GIsci Remote Sens, vol. 55, no. 1, pp. 1–18, Jan. 2018, doi: 10.1080/15481603.2017.1354803.

[37] J. W. van Wagtendonk, R. R. Root, and C. H. Key, “Comparison of AVIRIS and Landsat ETM+ detection capabilities for burn severity,” Remote Sens Environ, vol. 92, no. 3, pp. 397–408, Aug. 2004, doi: 10.1016/j.rse.2003.12.015.

[38] L. B. Lentile et al., “Remote sensing techniques to assess active fire characteristics and post-fire effects,” Int J Wildland Fire, vol. 15, no. 3, p. 319, 2006, doi: 10.1071/WF05097.

[39] A. Trucchia et al., “PROPAGATOR: An Operational Cellular-Automata Based Wildfire Simulator,” Fire, vol. 3, no. 3, p. 26, Jul. 2020, doi: 10.3390/fire3030026.

[40] J. Ramirez and A. de Santis, “The Next Step of Remote Sensing Services for Operational Forest Fire-Fighting within GMES masterFUEGO. Advanced training in Wildland Fire Science and Integrated Management View project FSD-Swiss Foundation for Humanitarian Demining,” 2006. [Online]. Available: https://www.researchgate.net/publication/259800361

[41] J. A. Morgan and J. F. Tatar, “Calculation of the Residual Sum of Squares for all Possible Regressions,” Technometrics, vol. 14, no. 2, pp. 317–325, May 1972, doi: 10.1080/00401706.1972.10488918.

[42] S. Trigg and S. Flasse, “An evaluation of different bi-spectral spaces for discriminating burned shrub-savannah,” Int J Remote Sens, vol. 22, no. 13, pp. 2641–2647, Jan. 2001, doi: 10.1080/01431160110053185.

[43] L. Schepers, B. Haest, S. Veraverbeke, T. Spanhove, J. vanden Borre, and R. Goossens, “Burned Area Detection and Burn Severity Assessment of a Heathland Fire in Belgium Using Airborne Imaging Spectroscopy (APEX),” Remote Sens (Basel), vol. 6, no. 3, pp. 1803–1826, Feb. 2014, doi: 10.3390/rs6031803.

[44] D. van Dijk, S. Shoaie, T. van Leeuwen, and S. Veraverbeke, “Spectral signature analysis of false positive burned area detection from agricultural harvests using Sentinel-2 data,” International Journal of Applied Earth Observation and Geoinformation, vol. 97, p. 102296, May 2021, doi: 10.1016/j.jag.2021.102296.

[45] C. Evangelides and A. Nobajas, “Red-Edge Normalised Difference Vegetation Index (NDVI705) from Sentinel-2 imagery to assess post-fire regeneration,” Remote Sens Appl, vol. 17, p. 100283, Jan. 2020, doi: 10.1016/j.rsase.2019.100283.

[46] “User Guides - Sentinel-2 MSI - Sentinel Online - Sentinel Online.” https://sentinel.esa.int/web/sentinel/user-guides/sentinel-2-msi (accessed Oct. 29, 2022).

[47] I. Argentiero et al., “Combining methods to estimate post-fire soil erosion using remote sensing data,” Forests, vol. 12, no. 8, Aug. 2021, doi: 10.3390/f12081105.

[48] H. Arefi, F.-J. Behr, and F. Alidoost, Geoinformation-Supporting Crisis and Disaster Management School of Surveying and Geospatial engineering.

[49] S. A. Shah, D. Z. Seker, S. Hameed, and D. Draheim, “The Rising Role of Big Data Analytics and IoT in Disaster Management: Recent Advances, Taxonomy and Prospects,” IEEE Access, vol. 7, pp. 54595–54614, 2019, doi: 10.1109/ACCESS.2019.2913340.

[50] M. S. Tehrany, B. Pradhan, and M. N. Jebur, “Flood susceptibility analysis and its verification using a novel ensemble support vector machine and frequency ratio method,” Stochastic Environmental Research and Risk Assessment, vol. 29, no. 4, pp. 1149–1165, May 2015, doi: 10.1007/s00477-015-1021-9.

[51] I. R. Widiasari, L. E. Nugroho, and Widyawan, “Deep learning multilayer perceptron (MLP) for flood prediction model using wireless sensor network based hydrology time series data mining,” in 2017 International Conference on Innovative and Creative Information Technology (ICITech), Nov. 2017, pp. 1–5. doi: 10.1109/INNOCIT.2017.8319150.

[52] S. Saravi, R. Kalawsky, D. Joannou, M. Rivas Casado, G. Fu, and F. Meng, “Use of Artificial Intelligence to Improve Resilience and Preparedness Against Adverse Flood Events,” Water (Basel), vol. 11, no. 5, p. 973, May 2019, doi: 10.3390/w11050973.

[53] N. Anusha and B. Bharathi, “Flood detection and flood mapping using multi-temporal synthetic aperture radar and optical data,” The Egyptian Journal of Remote Sensing and Space Science, vol. 23, no. 2, pp. 207–219, Aug. 2020, doi: 10.1016/j.ejrs.2019.01.001.

[54] “Platform – Google Earth Engine.” https://earthengine.google.com/platform/ (accessed Oct. 29, 2022).

[55] C. W. , L. P. J. Y. A. S. S. K. W. J. and N. P. H. Ross, “Global Hydrologic Soil Groups (HYSOGs250m) for Curve Number-Based Runoff Modeling”.

[56] “CLC 2018 — Copernicus Land Monitoring Service.” https://land.copernicus.eu/pan-european/corine-land-cover/clc2018 (accessed Nov. 14, 2022).

[57] “SardegnaMappe.” https://www.sardegnageoportale.it/webgis2/sardegnamappe/?map=download_raster (accessed Oct. 31, 2022).